

NANOMEDICINE-MEDIATED REPROGRAMMING  
OF TUMOR IMMUNOGENICITY

by

Emilio Jose Lara, B.S.

A thesis submitted to the Graduate Council of  
Texas State University in partial fulfillment  
of the requirements for the degree of  
Master of Science  
with a Major in Biochemistry  
August 2021

Committee Members:

Tania Betancourt, Chair

Wendi David

Liqin Du

**COPYRIGHT**

by

Emilio Jose Lara

2021

## **FAIR USE AND AUTHOR'S PERMISSION STATEMENT**

### **Fair Use**

This work is protected by the Copyright Laws of the United States (Public Law 94-553, section 107). Consistent with fair use as defined in the Copyright Laws, brief quotations from this material are allowed with proper acknowledgement. Use of this material for financial gain without the author's express written permission is not allowed.

### **Duplication Permission**

As the copyright holder of this work I, Emilio Jose Lara, refuse permission to copy in excess of the "Fair Use" exemption without my written permission.

## **DEDICATION**

To

My amazing wife and my best friend, Victoria, who supported me every step of the way  
and was always there to pick me up and encouraged me to keep going. Without her  
unconditional love, none of this would have been possible.

Thank you for always believing in me.

That's why we're a great team.

My daughters, Carolina and Elliana, who's love motivated me to be and do better.  
You girls are my world.

The first superhero in my life, my mom, who I always looked up to and admired.  
Te quiero mucho, mama!

## **ACKNOWLEDGEMENTS**

I would like to thank the people without whom I would not have been able to get to where I am today.

First of all, I would like to acknowledge and thank my amazing advisor, Dr. Tania Betancourt. I am fortunate to have been part of your lab and had you as my mentor. I truly appreciate every opportunity you encouraged me to pursue because they have all helped me grow as a scientist. I want to thank you for giving me the chance to be trained in so many techniques; an opportunity that I don't believe I would've received anywhere else. I also want to thank you for always being so supportive, understanding, and sharing your knowledge with me. I attribute the success I achieved during my undergraduate and graduate years to you. I cannot express how grateful I am for your guidance which has helped shape not only my future but the future of my family. Thank you, Dr. Betancourt, for being the awesome mentor that you are.

I would like to acknowledge our collaborators, Dr. Jennifer Irvin, Dr. James Tunnell, and Dr. Wendi David. I also want to thank my advisory committee members, Dr. Liqin Du and Dr. Wendi David for their valuable feedback on my project. I would like to especially thank Dr. Ryan Peterson for allowing us to utilize the flow cytometer in his lab.

I would like to thank all of the members in the Betancourt Research Laboratory both undergraduate and graduate students who have been awesome lab mates and who will be continuing my work. I would like to give a huge shout out to the nicest

kindhearted person I've ever met, Dr. Niloofar Heshmati. Thank you for being a great friend, taking time to teach and train me, collaborating and helping me as much as you did. Thank you Dami Runsewe for all of your advice, sharing your experiences, and for all the great conversations. I also want to thank past members in the Betancourt lab, Travis Cantu, Madeline Huff, and Fatma Gokmen whose work was important to my research.

## TABLE OF CONTENTS

	<b>Page</b>
ACKNOWLEDGEMENTS .....	v
LIST OF FIGURES .....	ix
ABSTRACT .....	x
CHAPTER	
1. INTRODUCTION .....	1
1.1 Objective .....	1
2. BACKGROUND .....	4
2.1 Immune Checkpoint Therapy .....	4
2.2 Immunogenic Cell Death .....	6
2.3 Polymeric Nanomedicine .....	8
2.4 Photothermal Therapy .....	10
3. MATERIALS AND METHODS .....	15
3.1 Materials .....	15
3.2 Nanoparticle (NP) Synthesis .....	16
3.3 Nanoparticle Characterization .....	18
3.4 Laser-Induced Photothermal Effect of PEDOT NPs .....	18
3.5 Cell Culture .....	19
3.6 Cell Internalization of NPs .....	21
3.7 Effect of PEDOT NP-PTT on Cell Death .....	22
3.8 Induction of Immunogenic Cell Death (ICD) via PEDOT NP-PTT .....	23
3.9 Activation of Dendritic Cells (DCs) .....	25
4. RESULTS .....	27
4.1 Characterization of PEDOT and PEDOT/NR NPs .....	27
4.2 Analysis of PEDOT NPs as Photothermal Agents .....	29
4.3 Intracellular Localization of PEDOT NPs .....	31

4.4 Qualitative Analysis of Cell Death by MTT Assay .....	32
4.5 Presentation of Damage Associated Molecular Patterns (DAMPs) ...	33
4.6 Dendritic Cell (DC) Activation .....	37
5. DISCUSSION AND CONCLUSION .....	39
5.1 Discussion .....	39
5.2 Conclusion .....	42
APPENDIX SECTION .....	43
REFERENCES .....	45

## LIST OF FIGURES

<b>Figure</b>	<b>Page</b>
1. Blockade of CTLA-4 Immune Checkpoint .....	6
2. Fluorescence microscopy images of MDA-MB-231 cells exposed to 500 $\mu\text{m}/\text{mL}$ PEDOT NPs (fluorescently labeled with Nile Red) for 1.5 and 24 hours .....	12
3. Fluorescence microscopy image of cells exposed to NPs for 6 h and irradiated with an 808-nm laser .....	13
4. Fluorescence microscopy image of MDA-MB-231 cells exposed to 500 $\mu\text{g}/\text{mL}$ PEDOT NPs for 1.5 h and irradiated with an 808-nm laser .....	14
5. Oxidative-emulsion polymerization method used for PEDOT NP preparation .....	17
6. Custom-built incubator for laser-induced PTT studies .....	20
7. PEDOT NP characterization .....	28
8. PEDOT/NR NP characterization .....	28
9. Temperature ( $^{\circ}\text{C}$ ) change over 15 min time period .....	30
10. Laser scanning confocal microscopy images of B16-F10 melanoma cancer cells incubated with PEDOT/NR NPs at a 500 $\mu\text{g}/\text{mL}$ concentration for 1.5 h .....	32
11. B16-F10 cell viability as a function of time .....	33
12. Flow cytometry histograms .....	35
13. Amount of HMGB1 (ng/mL) detected in cell media after 5-, 10-, and 15-min laser irradiation .....	36
14. Fluorescence intensities of DC markers .....	38

## ABSTRACT

Cancer is the second leading cause of death in the United States and has a major impact on our society. Melanoma is listed as one of the top leading cancers in men and women and was expected to account for 6,850 cancer deaths in 2020. Many treatment options exist but are accompanied with adverse side effects that can halt treatments. Immune checkpoint therapy is a novel approach in our fight against cancer and one that earned James P. Allison and Tasuko Honjo the 2018 Nobel Prize in Physiology or Medicine for their discovery of cancer therapy by inhibition of negative immune regulation. While immune checkpoint therapy has proven effective in the treatment of metastatic melanoma, this success has been limited to a small fraction of patients. The reason for low response rates is thought to be due to tumor intrinsic factors that alter the tumor microenvironment and allow tumor cells to evade destruction by dysregulating T cell function. The goal of this research was to investigate the utilization of poly(3,4-ethylenedioxythiophene) (PEDOT) nanoparticle-assisted photothermal therapy (PEDOT NP-PTT) for ablation of B16-F10 melanoma cells in order to evaluate their ability to convert nonimmunogenic tumors to immunogenic ones that will respond to immune checkpoint therapy. To accomplish these goals, the following objectives were pursued: preparation and characterization of nanoparticles, demonstration of the therapeutic effect of PEDOT NP-PTT, evaluation of the induction of immunogenic cell death following treatment, and evaluation of the extent of dendritic cell activation upon PTT through an *in vitro* assay.

## **1. INTRODUCTION**

### **1.1 Objective**

Cancer has been reported as the second leading cause of death in the United States.<sup>1,2</sup> It was estimated that there was approximately 606,520 cancer deaths and 1,806,590 new cancer diagnosis in the U.S. in 2020.<sup>3</sup> From these estimates, melanoma of the skin was expected to account for 1.1% of cancer deaths (6,850) and 5.6% of new cancer diagnosis (100,350).<sup>3</sup> Melanoma is listed as the fifth and sixth leading cancer in men and women, respectively, with the probability of 1 in 28 men and 1 in 41 women developing melanoma in their lifetime.<sup>3</sup> A few factors that affect your chances of developing melanoma include age, sex, ethnicity, and exposure to harmful ultraviolet radiation. Depending on the stage and location of the cancer, current treatment options for melanoma include surgery, chemotherapy, radiation therapy, targeted therapy, and immunotherapy, either alone or in combination. Surgery is the main treatment option for most melanomas and is often curative in early diagnosis.<sup>4</sup> Although these therapies have proven effective in some cases, low specificity for tumor cells, adverse side effects, and drug resistance are major challenges faced in melanoma therapy.<sup>5,6</sup>

Immune checkpoint (ICP) therapy has provided a new approach in the battle against cancer by utilizing antibodies to target immune inhibitory pathways involved in T cell regulation.<sup>7</sup> In the treatment of metastatic melanoma, a subset of patients treated with ICP therapy experienced durable responses and long-term survival over 10 years.<sup>7</sup> The reason for low response rates is thought to be due to tumor-intrinsic factors that alter the tumor microenvironment and allow tumor cells to evade destruction by dysregulating

T cell function.<sup>8</sup>

The long-term goal of this research was to investigate the utilization of poly(3,4-ethylenedioxythiophene) (PEDOT) nanoparticle (NP)-assisted photothermal therapy (PEDOT NP-PTT) for ablation of B16-F10 melanoma cells in order to evaluate their ability to convert nonimmunogenic tumors to immunogenic ones that will respond to ICP therapy. Specific goals of this project were the use PEDOT NPs as photothermal therapy (PTT) agents to induce immunogenic cell death (ICD) in melanoma cells upon PTT laser and to modulate *in vitro* dendritic cell (DC) activation. The hypothesis of this research was that the release of immunogenic damage-associated molecular patterns (DAMPs) from cancer cells undergoing ICD as a result of PEDOT NP-PTT would lead to activation of DCs.

To accomplish these goals, the following objectives were achieved:

**1. Preparation and characterization of PEDOT NPs.** PEDOT NPs were synthesized from the monomer 3,4-ethylenedioxythiophene (EDOT) using an oxidative-emulsion polymerization method similar to that reported by Cantu *et al.* and Huff *et al.* from our laboratory.<sup>9, 10</sup>

**2. Demonstration of therapeutic effect of PEDOT NP-PTT.** The cellular metabolic activity was measured to qualitatively assess the resulting level of cell death as a function laser irradiation. Following exposure to PEDOT NPs and irradiation with a NIR laser, the 3-(4,5-dimethyltiazol-2-yl)-2,5-diphenyl-2H-tetrazolium bromide (MTT) colorimetric assay was conducted to determine the percent of viable cells.

**3. Evaluation of the induction of immunogenic cell death (ICD) after**

**PEDOT NP-PTT.** The presence of damage-associated molecular patterns (DAMPs) following PEDOT NP-PTT were quantitatively analyzed. Enzyme-linked immunosorbent assay (ELISA) was carried out for the detection of released high-mobility group box 1 (HMGB1). Flow cytometry was conducted for the detection of calreticulin (CRT), heat-shock protein 70 (HSP70), and heat-shock protein 90 (HSP90).

**4. Evaluation of the extent of dendritic cell activation upon PTT through *in vitro* assay.** Following PEDOT NP-PTT, treated cancer cells were co-cultured with immature DCs using a transwell co-culture system that allows media to be shared between the treated melanoma cells and DCs. DC markers CD11c, CD86, and CD80 present on the surface of mature DCs were fluorescently labeled and quantitative analysis was conducted by flow cytometry.

## **2. BACKGROUND**

### **2.1 Immune Checkpoint Therapy**

Research in cancer immunology has provided us with a better understanding of the mechanisms involved in regulating immune responses. This led to the development of biological drugs, typically antibodies, used in immune checkpoint (ICP) therapies that target T cell inhibitory pathways to unleash anti-tumor immune response.<sup>11</sup> ICP therapy is a novel approach in our fight against cancer and one that earned James P. Allison and Tasuko Honjo the 2018 Nobel Prize in Physiology or Medicine for their discovery of cancer therapy by inhibition of negative immune regulation. In 2011, ipilimumab (trade name Yervoy) became the first ICP agent to gain FDA approval for the treatment of metastatic melanoma. Ipilimumab is a monoclonal antibody that targets cytotoxic T-lymphocyte antigen-4 (CTLA-4), a protein receptor expressed on regulatory T cells that functions as an immune checkpoint. When bound to the B7-1 ligand of tumor cells, CTLA-4 downregulates T-cell response.<sup>7</sup> Ipilimumab (anti-CTLA-4) blocks this inhibitory pathway allowing T cells to identify and destroy tumor cells (Figure 1).<sup>12</sup>

Another identified and widely studied immune checkpoint pathway is that of programmed cell death-1 (PD-1) and programmed death-ligand 1 (PD-L1). Similarly to CTLA-4, PD-1 is expressed on regulatory T cells and function to maintain peripheral tolerance. Tumor cells upregulate PD-L1, inhibiting antitumor T cell response. ICP agents pembrolizumab and nivolumab (anti-PD-1) and atezolizumab (anti-PD-L1), all FDA approved antibodies, block the PD-1/PD-L1 pathway to increase antitumor response.<sup>13</sup> Many more inhibitory checkpoint pathways have been identified and

hundreds of ICP agents are currently in clinical trials.<sup>14</sup>

While ICP therapy has proven effective, this success has been limited to a small fraction of patients. Several tumor intrinsic mechanisms have been identified that function in the expression or repression of certain proteins on tumor cells and are believed contribute to tumor resistance to ICP therapy.<sup>15</sup> These mechanisms lead to a “nonimmunogenic” tumor microenvironment. The use of combinatorial therapeutic strategies such (e.g. ICP combined with localized hyperthermia) has been suggested as a way to increase response rates.<sup>7,10,16</sup> Specifically, the use of therapies that lead to ICD is hypothesized to transform a nonimmunogenic microenvironment into an immunogenic one that can respond to ICP. In this work, the use of NP-PTT as a method to induce ICD in treated cancer cells and induce the maturation of DCs, the first two steps required to elicit an adaptive immune response to cancer antigens, was investigated.

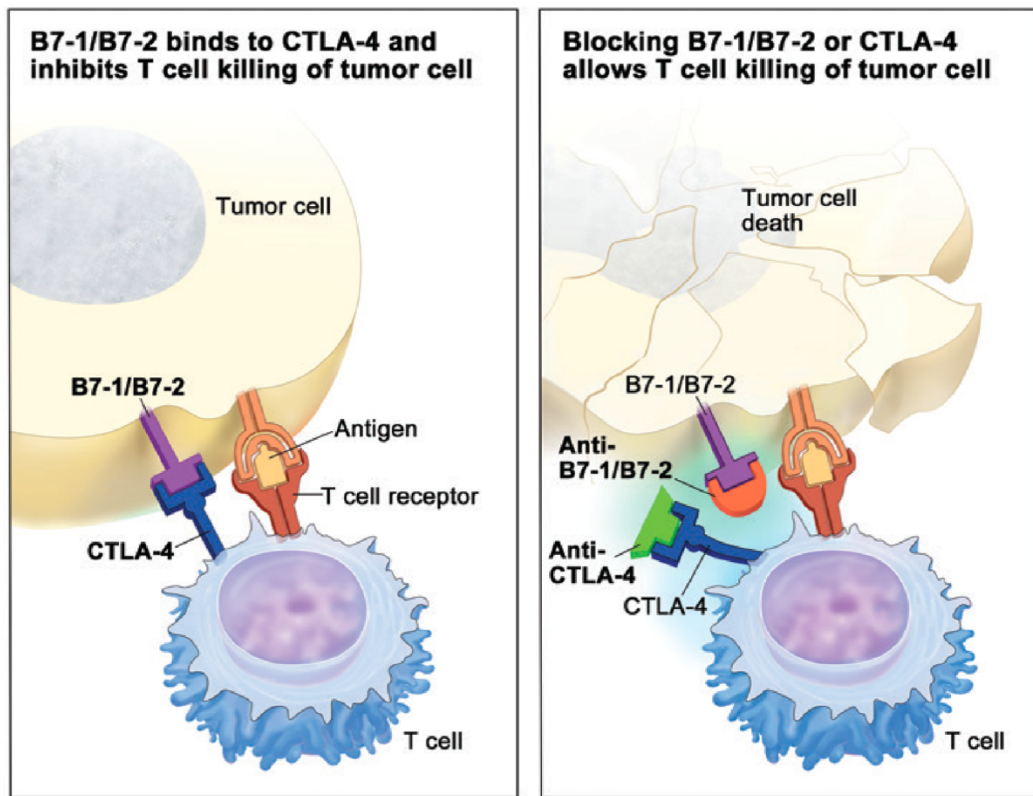


**Figure 1.** Blockade of CTLA-4 Immune Checkpoint. Upregulation of B7-1/B7-2 ligand by tumor cell downregulates T cell function and evades destruction (left). Anti-CTLA-4 inhibitor blocks the binding of B7-1/B7-2 to CTLA-4, T cells are able to identify and destroy tumor cells (right).<sup>11</sup>

## 2.2 Immunogenic Cell Death

Regulated cell death, or apoptosis, is a critical biological process for all multicellular organisms. This essential mechanism regulates tissue homeostasis, immune regulation, and the destruction of damaged cells.<sup>16</sup> Apoptosis is a normal part of the cell cycle with the programmed death of a cell being genetically determined. It involves a coordinated and complex cascade of ATP-dependent molecular events that can be initiated by a variety of internal or external stimuli which ultimately lead to cell death.<sup>16</sup> Cancer cells fail to undergo apoptosis which results in unregulated cell growth.<sup>17</sup>

Immunogenic cell death (ICD) is a form of regulated cell death that can initiate an adaptive immune response specific for cellular or viral antigens expressed by apoptotic cells.<sup>18</sup> Apoptotic cells can either release to the extracellular space or present on their cell membrane damage-associated molecular patterns (DAMPs) which act as ‘danger’ signals to produce an immune response.<sup>19</sup> DAMPs interact with antigen presenting cells, such as dendritic cells (DCs), or other immune cells. These molecules include calreticulin (CRT), ATP, high-mobility group box 1 (HMGB1), heat-shock protein 70 (HSP70), and heat-shock protein 90 (HSP90).<sup>19</sup>

Apoptotic cells translocate CRT from the perinuclear endoplasmic reticulum, where it maintains Ca<sup>2+</sup> homeostasis, to the outer cell membrane, serving as a signal to promote phagocytosis by DCs.<sup>20</sup> The extracellular release of ATP is another hallmark of ICD which occurs during the blebbing phase of apoptosis and acts as a chemoattractant for DC precursors.<sup>21</sup> HMGB1, a non-histone chromatin binding protein, is translocated from the nucleus to the extracellular surface in the late stages of apoptosis.<sup>22,23</sup> Reports have shown that the binding of HMGB1 to Toll-like receptor 4 (TLR4), expressed in DCs, is essential for DC activation.<sup>24</sup> HSP70 and HSP90 are upregulated help to stabilize cells from thermal and oxidative stress and are also a characteristic of ICD.<sup>25</sup>

ICD can be initiated by stimuli from viral infections, as well by some chemotherapeutic agents (e.g. anthracyclines, bortezomib), hypericin-based photodynamic therapy, Prussian blue NP-mediated photothermal therapy, and various other anti-cancer therapeutic modalities.<sup>18,26,27</sup> In this work, we investigated if NP-PTT using PEDOT NPs leads to ICD in melanoma cells by studying the relative levels of CRT, HMGB1, HSP70 and HSP90 presented on the cell surface or released to the cell

medium after treatment.

### **2.3 Polymeric Nanomedicine**

Advances in nanotechnology gave rise to the medical research field of nanomedicine which focuses the development NPs for therapeutic and diagnostic applications. Various nanomedicines have been introduced and many are being developed for cancer treatment and diagnosis. Polymeric NPs can be synthesized from natural or synthetic polymers and designed to exhibit different physicochemical properties such as size, shape, and surface properties. NPs can vary in size and range between 1 to 1000 nm. Their physicochemical properties are important in governing their application and efficiency.<sup>28</sup>

For therapeutic applications, NPs are mainly used as drug delivery systems that target tumors and release therapeutic agents at the pathological site. The goal of therapeutic NPs are to increase therapeutic efficacy and reducing drug toxicity that can lead to adverse side effects, a limiting factor in conventional cancer treatments such as chemotherapy.<sup>29</sup> The tumor specificity property of therapeutic NPs is due a process called the enhanced permeability and retention (EPR) effect. This effect leads to the accumulation and retention of nanoparticles in solid tumor tissue for a prolonged time.<sup>30</sup> Healthy tissues contain blood vessel lined with organized structured endothelial cells that prevent large macromolecules or particles from diffusing into normal tissue, as well as a lymphatic drainage system that removes extracellular fluid leaked into normal tissues, thereby preventing possible tissue damage. Tumor tissues are abnormal in architecture,

with poorly aligned endothelial cells and lack a properly functioning lymphatic system. NPs are able to pass through the gaps between the misaligned endothelial cells and, due to the lack of a functional lymphatic drainage system, are retained within the tumor tissue for a prolonged time period.<sup>31</sup> However, to exploit the EPR effect, NPs must be between 10 to 100 nm in size to be able to diffuse through the endothelium of tumor tissues.<sup>30,32,33</sup>

For diagnostic applications, NPs formulations have been developed as contrast agents for bioimaging. Magnetic NPs, NPs containing iron oxide or gadolinium derivatives, have shown to be effective contrast agents for MRI due to their enhanced proton relaxation capabilities.<sup>34</sup> Several MRI contrast agents containing magnetic NPs have been FDA-approved for clinical use. Gastrograph (ferumoxsil) is an oral suspension containing superparamagnetic iron oxide NPs (SPIONs) and is used as a bowel contrast agent.

Doxil and Abraxane are two noteworthy examples of FDA approved nanomedicines that have demonstrated clinical success for the treatment of cancer.<sup>35</sup> Doxil, a liposomal nanoformulation of doxorubicin, gained FDA approval in 1995 for the treatment of AIDS-related Kaposi's sarcoma but has since been approved to treat ovarian cancer and multiple myeloma. Abraxane, an albumin-bound nanoformulation of paclitaxel, gained FDA approval in 2005 for the treatment of metastatic breast cancer and was later for the treatment of lung and pancreatic cancer. These two nanomedicines are particularly notable because due to their nanoformulation, they are able to better target tumor tissue through the EPR effect and reduce drug toxicity experienced in conventional doxorubicin and paclitaxel treatment which had limited their use.<sup>31</sup> Although adverse side effects were reduced, these new formulations did not produce significant

improvements in therapeutic index. Recent data shows that while promising results have been reported in treating tumors in mouse models using nanomedicines, they fail to translate in patient care.<sup>36</sup>

In this work, conductive polymer PEDOT nanoparticles were utilized for cancer therapy via photothermal ablation, a highly specific therapeutic method described in the next subsection.

## 2.4 Photothermal Therapy

PTT has been widely studied as an alternative method for the treatment of cancer. This highly selective and effective treatment works by exposing cancer cells to hyperthermia, temperature range of 41-50 °C, and allows for minimal damage to the surrounding normal tissues.<sup>37,38</sup> Compared to normal tissue, tumor cells have a low heat tolerance and are destroyed in this temperature range.<sup>39</sup> PTT agents are able to absorb light in the near infrared (NIR) region (700-900 nm) and release the absorbed energy in the form of heat.<sup>40</sup> A variety of NPs have been evaluated for the use in photothermal treatment of cancer and many have had successful therapeutic results, including gold nanoshells and nanorods NPs, iron oxide NPs, silica NPs, carbon nanotubes, and conductive polymer NPs.<sup>9,41-45</sup> In NP-PTT, tumor cells are treated with a PTT agent in the form of a NP. The PTT agents are then irradiated with near infrared (NIR), resulting in localized release of energy as heat, which can significantly stress or kill cancer cells via protein denaturation, induction of apoptosis, or necrosis.<sup>38</sup> Our laboratory has previously demonstrated conductive polymer poly(3,4-ethylenedioxythiophene)

(PEDOT) NPs (<100 nm) to be effective photothermal agents in the ablation of MDA-MB-231 breast cancer cells.<sup>9</sup> These nanoparticles were found to have a greater than 50% photothermal conversion efficiency upon irradiation with a 808-nm laser, to be very stable in aqueous solutions, and, importantly, to be cytocompatible at therapeutic concentrations.<sup>9</sup> In addition, we have shown PEDOT NPs to be readily internalized (Figure 2) and to induce either apoptosis or necrosis, depending on NP concentration and laser irradiation dose (Figure 3), in MDA-MB-231 breast cancer cells.<sup>10</sup> Finally, our laboratory has also shown that PEDOT NP-PTT can induce ICD in these cells, as shown by calreticulin presentation on the cell surface (Figure 4), and HMGB1 decrease inside the cells (data not shown).<sup>10</sup>

In the proposed work, the ability of PEDOT NPs as NP-PTT to mediate a therapeutic effect and induce ICD was investigated in the B16-F10 murine melanoma cell model. In addition, the maturation of DCs upon interaction with cancer cell-specific antigens and DAMPs was studied.

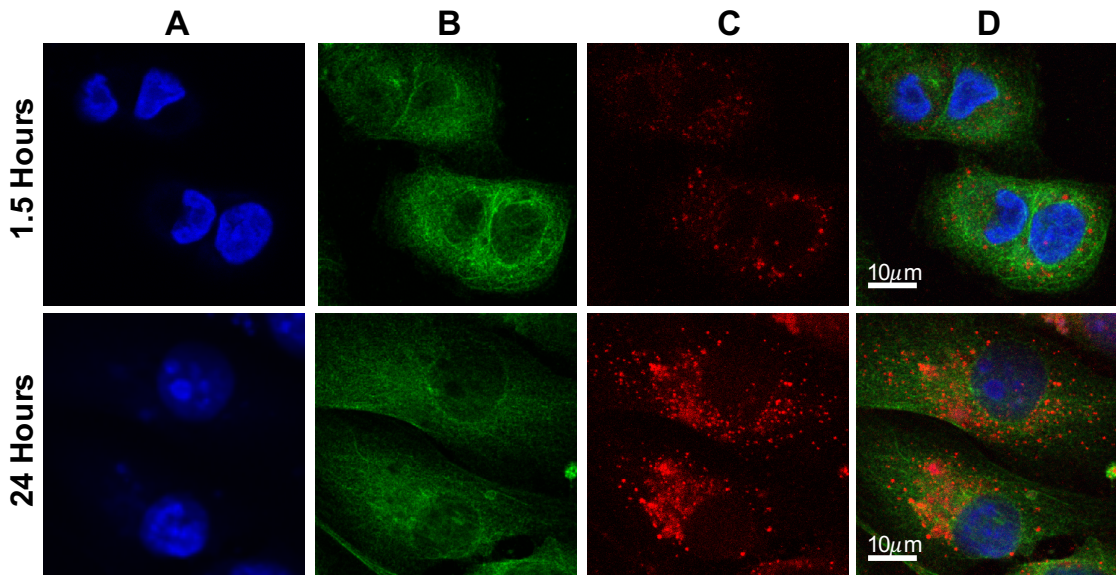


**Figure 2.** Fluorescence microscopy images of MDA-MB-231 cells exposed to 500  $\mu\text{m}/\text{mL}$  PEDOT NPs (fluorescently labeled with Nile Red) for 1.5 and 24 hours. Stains: (A) nucleus (DAPI), (B) tubulin (anti-tubulin monoclonal antibody + anti-IgG Dylight 488 polyclonal antibody), (C) NPs (Nile Red), and (D) overlay.<sup>10</sup>

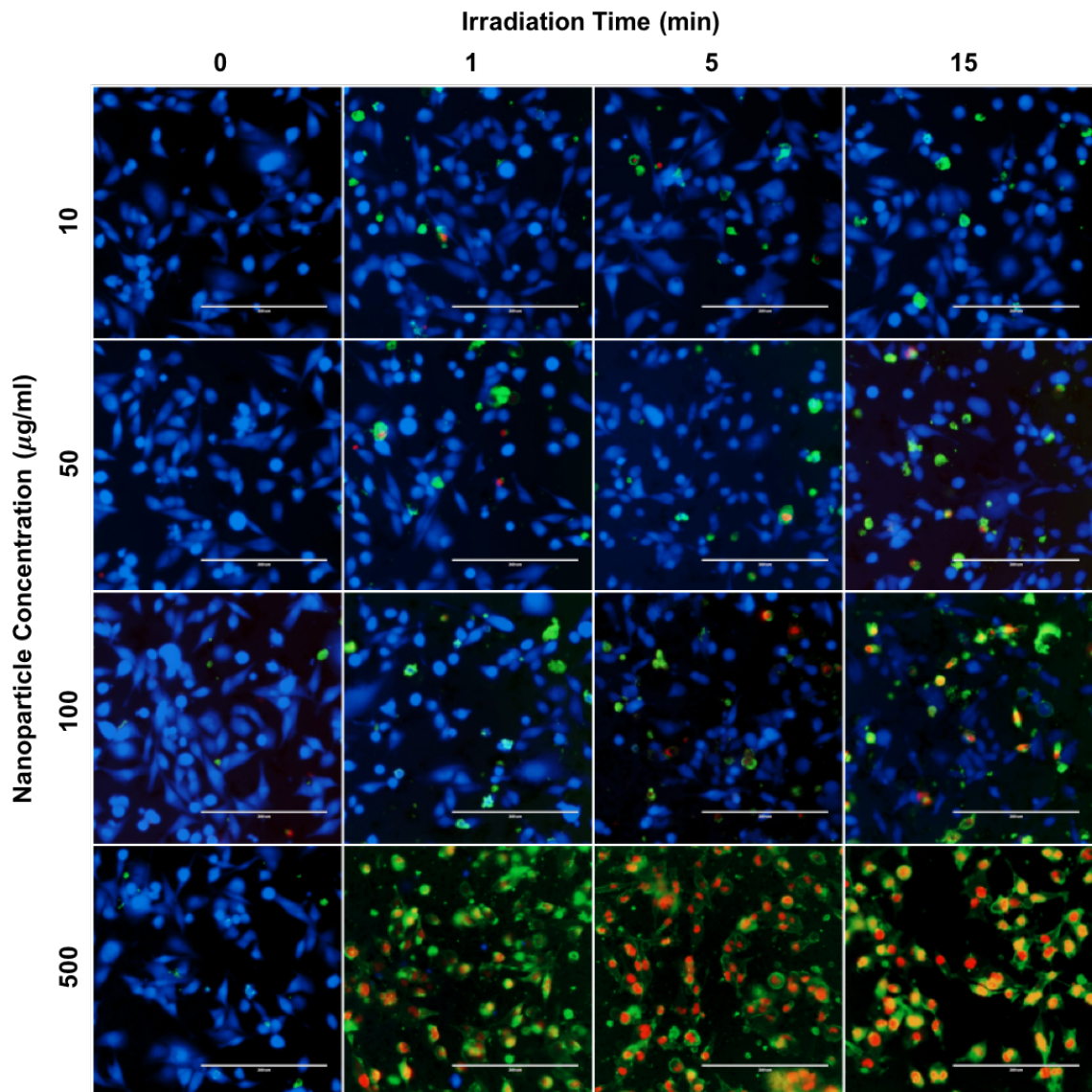


**Figure 3.** Fluorescence microscopy image of cells exposed to NPs for 6 h and irradiated with an 808-nm laser. Cells were exposed to 10, 50, 100, and 500  $\mu\text{g}/\text{mL}$  NP concentrations for 0, 1, 5, and 15 min irradiation time periods. Blue fluorescence represents live cells (Calcein Blue), green fluorescence represents apoptotic cells (Annexin V AlexaFluor 448), and red fluorescence represents necrotic cells (Propidium Iodide). Scale bar = 200  $\mu\text{m}$ .<sup>10</sup>

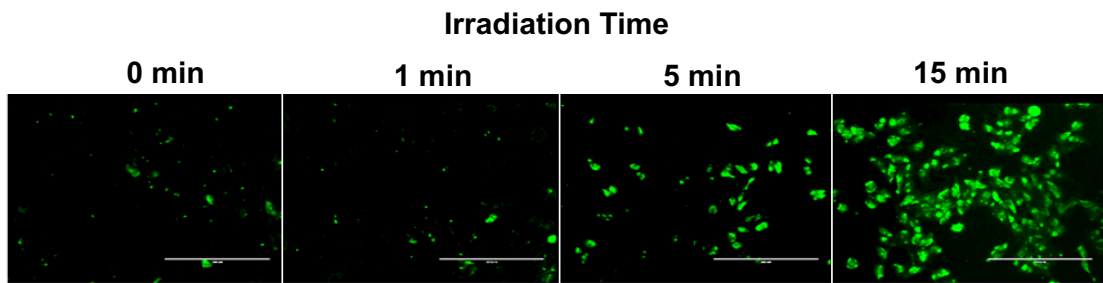


**Figure 4.** Fluorescence microscopy image of MDA-MB-231 cells exposed to 500  $\mu\text{g/mL}$  PEDOT NPs for 1.5 h and irradiated with an 808-nm laser. Green fluorescence represents calreticulin presentation on the cell surface after varying laser irradiation times. Scale bar = 200  $\mu\text{m}$ .<sup>10</sup>

### **3. MATERIALS AND METHODS**

#### **3.1 Materials**

3,4-Ethylenedioxythiophene (EDOT), poly(4-styrenesulfonic acid-*co*-maleic acid) (PSS-*co*-MA) sodium salt (20,000 Da, 3:1 styrenesulfonic acid: maleic acid), penicillin-streptomycin solution, albumin from bovine serum (BSA), and iron(III) chloride, were purchased from Sigma-Aldrich (St. Louis, MO, USA). 4-Dodecylbenzesulfonic acid (DBSA) was purchased from TCI America (Portland, OR, USA). Nile Red was obtained from Chem-Impex International, Inc. (Wood Dale, IL, USA). Triton X-100 was obtained from JT Baker, Inc., (Phillipsburg, NJ, USA). Thiazolyl blue tetrazolium bromide (MTT), 98%, was purchased from Alfa Aesar (Ward Hill, MA, USA). Rabbit anti-alpha tubulin monoclonal antibody (ab176560), rabbit anti-calreticulin polyclonal antibody (ab2907), rabbit anti-HMGB1 monoclonal antibody (ab79823), rabbit anti-HSP70 monoclonal antibody (ab181606), and rabbit anti-HSP90 monoclonal antibody (ab32568) were purchased from Abcam (Cambridge, England, UK). Goat anti-rabbit IgG (H&L) DyLight® 488 conjugate was purchased from ImmunoReagents, Inc. (Raleigh, NC, USA). HMGB1 Detection ELISA Kit (6010) was purchased from Chondrex, Inc. (Woodinville, WA, USA). 4',6-diamidino-2-phenylindole, dihydrochloride (DAPI) was purchased from MilliporeSigma (Burlington, MA, USA). Fluoromount-G was obtained from SouthernBiotech (Birmingham, AL, USA). Ultrapure deionized water (DI water) was obtained from a Millipore Direct-Q water purification system.

### 3.2 Nanoparticle (NP) Synthesis

Conductive poly(3,4-ethylenedioxythiophene) (PEDOT) nanoparticles (NPs) were prepared, as shown in Figure 5, via an oxidative-emulsion polymerization method equivalent to that reported by Cantu *et al.* and Huff *et al.*<sup>9,10</sup> Briefly, two liquid phases were prepared: an aqueous and organic phase. The aqueous phase consisted of a 1 mL solution composed of the surfactant poly(4-styrenesulfonic acid-*co*-maleic acid) (PSS-*co*-MA) sodium salt dissolved in ultrapure water at a concentration of 2% w/v and was prepared on a magnetic stir plate. The organic phase was prepared by making a 100  $\mu$ L solution containing the monomer 3,4-ethylenedioxythiophene (EDOT) (48 mg/mL) and 4-dodecylbenzesulfonic acid (DBSA) (0.3 mg/mL) dissolved in chloroform. To ensure homogeneity, the organic phase was mixed for 30 min. Afterwards, the organic phase was added dropwise in 20  $\mu$ L intervals to the aqueous phase under magnetic stirring. The emulsion was then diluted with 2 mL of ultrapure water. Next, 3.8  $\mu$ L of a 100 mg/mL aqueous solution of FeCl<sub>3</sub> (2.2 mol) was added and left for 1 h under magnetic stirring to allow polymerization to occur. The NPs were transferred to a 100-kDa molecular weight cutoff cellulose ester membrane (Spectrum Laboratories, 131420) and dialyzed for 17 h overnight. Lastly, the NPs were filtered through a sterile 0.2  $\mu$ M nylon membrane filter (Pall Corporation, 4433) for cell studies.

To determine the final PEDOT NP concentration, 1 mL of the PEDOT NP suspension was lyophilized for 48 h and the dry product was weighed.

For the purpose of visualizing the cellular uptake of NPs by melanoma cells, PEDOT NPs containing Nile Red (PEDOT/NR) were synthesized using the same oxidative-emulsion polymerization method described above, with one modification to the

organic phase. Briefly, 4 mM of Nile Red was dissolved in 100  $\mu$ L of toluene and was substituted for chloroform in the organic phase containing EDOT (48 mg/mL) and DBSA (0.3 mg/mL). All other steps were carried out as the same as above. PEDOT/NR NPs were dialyzed overnight for 17 h and the final concentration of the NPs was determined as before.

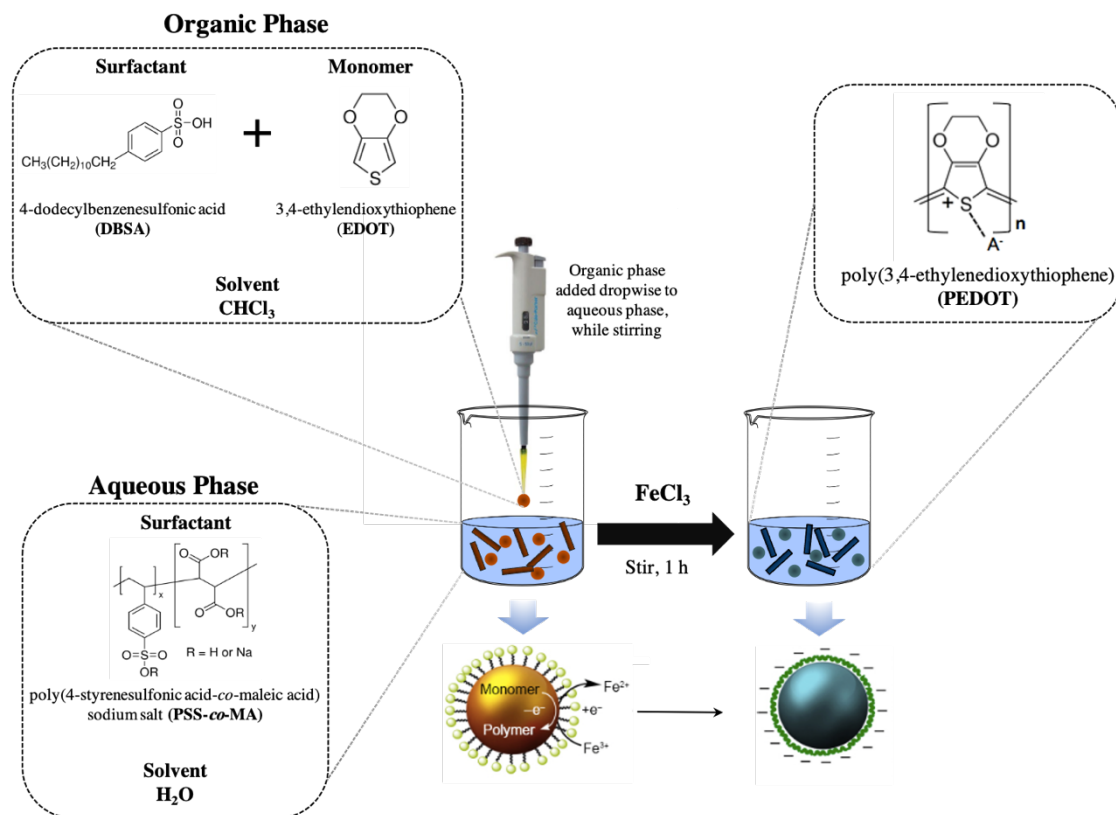


**Figure 5.** Oxidative-emulsion polymerization method used for PEDOT NP preparation.

### **3.3 Nanoparticle Characterization**

The diameter size and zeta potential of the PEDOT NPs was determined by dynamic light scattering (DLS) and electrophoretic light scattering (ELS) using a Malvern Zetasizer Nano ZS instrument. The diameter was determined by analyzing a polystyrene cuvette containing 450  $\mu$ L of the PEDOT NP suspension. Zeta potential analysis was carried out using a 1 mL sample composed of 950  $\mu$ L of 1 mM KCl solution and 50  $\mu$ L of the PEDOT NP suspension. UV/VIS/NIR absorption spectrophotometry was carried out using a Biotek Synergy H4 Hybrid Multi-Mode Microplate Reader to validate the PEDOT NPs ability to absorb light in the near-infrared (NIR) region.

### **3.4 Laser-Induced Photothermal Effect of PEDOT NPs**

NPs were irradiated using an 808-nm laser diode (RLCO-808-1000G, 9 mm; Roithner Lasertechnik GmbH, Wein, Austria) rated at 1 W of power. A laser power of 848 mW (irradiance = 3.0 W/cm<sup>2</sup>) was used and a biconvex lens (Thorlabs, Inc., Newton, NJ, USA) focused the laser diameter to 6 mm. All samples were placed 8 cm below the biconvex lens and irradiated in 96-well plates using 100  $\mu$ L of sample. A photosensitive VIS/NIR detector card (wavelength range: 400 to 640 nm and 800 to 1700 nm, Thorlabs Inc., Newton, NJ, USA) was used to facilitate locating the NIR laser beam and align the sample wells. The PEDOT NP suspension was diluted to 500  $\mu$ g/mL using complete cell media and irradiated for 5, 10, and 15 minutes. Complete cell media was used as a control. A Seek Shot™ thermal camera (Seek Thermal, Inc., Santa Barbara, CA, USA) was used to measure and visualize the temperature change of the samples.

### **3.5 Cell Culture**

Mouse B16-F10 melanoma cancer cells were obtained from American Type Culture Collection (ATCC) (Manassas, VA, USA) and cultured in a T-75 flask with complete cell growth media consisting of 88% 1X Dulbecco's Modification of Eagle's Medium (DMEM) (Corning, Corning, NY, USA) supplemented with 10% fetal bovine serum (FBS) (Corning Cellgro, Corning, NY, USA), 1% penicillin-streptomycin solution (Sigma Aldrich, St. Louis, MO, USA), and 1% L-glutamine solution (VWR, Radnor, PA, USA) incubated at 37 °C with 5% CO<sub>2</sub>. Once cells reached 80% confluency, cells were washed twice using 1X Dulbecco's Phosphate Buffered Saline (DPBS) without calcium and magnesium (Corning, Corning, NY, USA). The cells were detached using 0.25% trypsin-EDTA (1X) solution (Cytiva, Malborough, MA, USA), centrifuged at 125 RCF for 5 min, and resuspended in 5 mL of fresh cell media that was pre-warmed at 37 °C.

For PEDOT nanoparticle-mediated photothermal therapy (PEDOT NP-PTT), B16-F10 cells were seeded in 96-well plates using 100 μL sample volumes containing a cell density of 250,000 cells/well.

Mouse JAWSII immature dendritic cells (DCs) were obtained from ATCC (Manassas, VA, USA) and cultured in a T-25 flask with complete cell growth media consisting of 78.99% 1X Minimum Essential Medium (MEM) Alpha (Corning Cellgro, Corning, NY, USA) supplemented with 20% fetal bovine serum (FBS), 1% L-glutamine solution, and 0.01% recombinant murine granulocyte-macrophage colony-stimulating factor (GM-CSF) (PeproTech, Inc., Rocky Hill, NJ, USA), and were incubated at 37 °C with 5% CO<sub>2</sub>. Dendritic cells grow both attached and in suspension; therefore when changing media, 85% of the media was collected, centrifuged at 125 RCF for 10 min, and

cells pelleted were resuspended in 4.25 mL of pre-warmed fresh cell growth media. Once cells reached 80% confluence, cells were washed twice with 1X DPBS without calcium and magnesium, detached with 0.25% trypsin-EDTA (1X) solution, centrifuged at 125 RCF for 10 min, and resuspended in 5 mL of pre-warmed fresh cell growth media.

Laser-induced PTT studies were carried out in a custom-built incubator designed to maintain the cells in the optimal physiological temperature of 37 °C using an incandescent light bulb connected to a STC-1000 probe temperature controller (Figure 6).

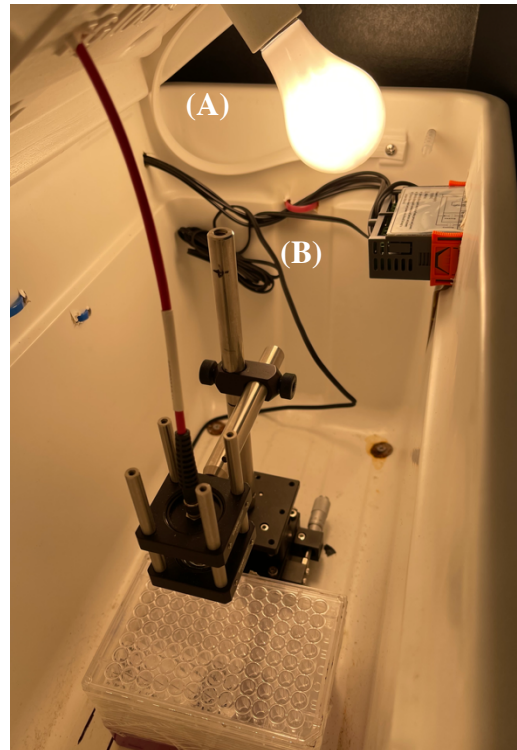


**Figure 6.** Custom-built incubator for laser-induced PTT studies. (A) Incandescent light bulb. (B) STC-1000 probe temperature controller.

### **3.6 Cell Internalization of NPs**

To view the internalization of PEDOT NPs in B16-F10 melanoma cancer cells, cells grown on a glass slide were treated, fixed, and fluorescently stained. Briefly, B16-F10 melanoma cancer cells were seeded in an 8-well glass slide (Lab-Tek® II Chamber Slide™, Thermo Fisher Scientific, Waltham, MA, USA) at a density of 150,000 cells/well and incubated at 37 °C for 24 h. Afterwards, the cell media was replaced with 300 µL of 500 µg/mL PEDOT/NR NPs and incubated for 1.5 h at 37 °C. After incubation, the cells were washed with cold DPBS. For fixation, cells were incubated in a 4% formaldehyde solution for 20 min at room temperature, then washed twice with 0.1% w/v BSA in 1X DPBS. To prevent nonspecific binding, cells were incubated at room temperature for 45 min in a blocking and permeabilizing buffer composed of 1% w/v BSA, 0.1% Triton X-100, and 22.5 mg/mL glycerol. The primary rabbit anti-alpha tubulin antibody (Abcam ab176560, 1:200 dilution in 0.1% w/v BSA) was then added and incubated at room temperature for 1 h, after which the cells were washed twice with 0.1% w/v BSA. The cells were then incubated with the secondary goat anti-rabbit IgG (H&L) DyLight® 488 conjugate (1:1000 dilution in 0.1% w/v BSA) in the dark for 1 h at room temperature, then washed twice with 0.1% w/v BSA. The cell nucleus was stained by incubating the cells with 1 µg/mL DAPI for 5 min, then the cells were rinsed with DI water. A slide separator and separator key were used per manufacturer to remove the 8-well media chambers from the glass slide. The slide was then carefully mounted on a glass cover slide containing 300 µL of Fluoromount-G and was analyzed using an Olympus® FLUOVIEW FV3000 confocal laser scanning microscope.

### **3.7 Effect of PEDOT NP-PTT on Cell Death**

Prior to PEDOT NP-PTT, B16-F10 melanoma cancer cells were seeded in 96-well plates containing 100  $\mu$ L sample volumes and a cell density of 10,000 cells/well. Cells were incubated at 37 °C for 24 h to allow cells to attach to the wells. Afterwards, the cell media was discarded and replaced with 100  $\mu$ L of PEDOT NPs diluted to a concentration of 500  $\mu$ g/mL using complete cell media containing DMEM without phenol red. The cells were then incubated at 37 °C for 1.5 h. To investigate the effect of laser irradiation time, cells were irradiated for 5, 10, and 15 min using an 808-nm laser diode with spot diameter of 6 mm and laser power of 0.85 W (3.0 W/cm<sup>2</sup>). Laser irradiation of cells was conducted with NPs in the media. Following laser irradiation, the cells were incubated for 30 min at 37 °C with 5% CO<sub>2</sub>. Controls included cells exposed to PEDOT NPs but not laser irradiation (0 min), cells that did not receive any treatment (NT), and cells treated with methanol (MeOH) for 15 min to induce cell death. All studies were performed in triplicate.

The MTT (3-[4,5-dimethylthiazol-2-yl]-2, 5 diphenyl tetrazolium bromide) viability assay was performed to analyze the effect of PEDOT NP-PTT on cell death. Metabolically active cells contain NADPH-dependent oxidoreductase enzymes that can reduce the yellow MTT reagent and convert it to purple formazan crystals which are soluble in DMSO. UV-VIS spectroscopy can be utilized to calculate the percent of viable cells using the resulting-colored solution. The color intensity of the solution is proportional to the amount of metabolically active cells or formazan concentration present. Following the 30 min incubation time after laser irradiation, 10  $\mu$ L of 5 mg/mL MTT reagent in cell media was added to the cells and allowed to incubate for 2 h at 37

$^{\circ}\text{C}$ . The cell media was then discarded and replaced with 200  $\mu\text{L}$  of DMSO. Formazan crystals were dissolved by gently pipetting the DMSO. Once dissolved, a Biotek H4 multimode plater reader was used to measure the optical density at 555 nm and 900 nm.

### **3.8 Induction of Immunogenic Cell Death (ICD) via PEDOT NP-PTT**

B16-F10 melanoma cells were transferred to microcentrifuge tubes at a cell density of 250,000 cells/tube and sample volumes of 1 mL. Cells were centrifuged at 150 rcf for 5 min at 15  $^{\circ}\text{C}$  and resuspended in 1 mL of PEDOT NP suspension in cell media at a concentration of 500  $\mu\text{g}/\text{mL}$ . After 1.5 h incubation at 37  $^{\circ}\text{C}$ , cells were centrifuged, resuspended in 100  $\mu\text{L}$  of pre-warmed fresh cell media, and transferred to 96-well plates. Cells were then irradiated for 5, 10, and 15 min using an 808-nm laser diode with spot diameter of 6 mm and laser power of 3.0  $\text{W}/\text{cm}^2$ . Following laser irradiation, the cells were incubated for 30 min at 37  $^{\circ}\text{C}$  with 5%  $\text{CO}_2$ . Controls included cells exposed to PEDOT NPs but not laser irradiation (NP control), cells that did not receive any treatment (NT), and cells without PEDOT NPs but exposed to 15 min laser irradiation (laser control).

The presence of DAMPs on the cells' membranes following PEDOT NP-PTT was investigated by flow cytometry which determined the level of surface bound heat-mobility group box 1 (HMGB1), calreticulin (CRT), heat-shock protein 70 (HSP70), and heat-shock protein 90 (HSP90). Flow cytometry is a widely used technique that utilizes laser-based technology to analyze the characteristics of cells or particles, such as cell size and granularity and is predominantly used to measure fluorescence intensity. The cell

suspensions are hydrodynamically focused in the cytometer causing cells to pass through a laser beam one at a time. Cells passing through the laser beam scatter light which is detected as forward and side scatter. Fluorescence emitted from positively stained cells are measured by fluorescence detectors. Briefly, after the 30 min incubation period at 37 °C following laser irradiation, the cells were transferred to microcentrifuge tubes and pelleted by centrifugation at 150 rcf for 5 min at 15 °C. The cells were washed with 1 mL DPBS (without Ca<sup>2+</sup> and Mg<sup>2+</sup>), centrifuged at 150 rcf for 5 min at 15 °C, then resuspended in 1 mL BSA (1% w/v) to block non-specific binding. After a 30 min incubation period, cells were centrifuged at 150 rcf for 5 min at 15 °C and the BSA solution was discarded. Four independent group of cells were incubated for 1 h at room temperature with either 50 µL of rabbit anti-HMGB1 monoclonal antibody (Abcam ab79823, 1:250 dilution in 0.1% w/v BSA), 50 µL of rabbit anti-CRT polyclonal antibody (Abcam ab2907, 1:75 dilution in 0.1% w/v BSA), 50 µL of rabbit anti-HSP70 monoclonal antibody (Abcam ab181606, 1:250 dilution in 0.1% w/v BSA), or 50 µL of rabbit anti-HSP90 monoclonal antibody (Abcam ab32568, 1:250 dilution in 0.1% w/v BSA). Following the 1 h incubation period, the cells were washed with 1 mL wash solution (DPBS with 0.1% w/v BSA), centrifuged at 150 rcf for 5 min, and the supernatant was discarded. Then, 50 µL of goat anti-rabbit IgG (H&L) DyLight® 488 conjugate (1:1000 dilution in 0.1% w/v BSA) was added and the cells were incubated in the dark for 1 h at room temperature. The cells were washed with 1 mL of wash solution, centrifuged at 150 rcf for 5 min, resuspended in 100 µL DPBS and analyzed by flow cytometry using a CytoFlex S Flow Cytometer (Beckman Coulter, Brea, CA, USA). Flow cytometry data was analyzed using the CytExpert software. The FITC channel was

selected to detect the fluorescence of the DyLight® 488 conjugate. For each sample, a total of 10,000 events were collected and histograms illustrating the fluorescent intensity against cell count were plotted. To avoid the effect of outliers, flow cytometry data was reported as the median  $\pm$  robust standard deviation (rSD). The rSD is based upon the deviation of individual data points to the median of the cell population.

The enzyme-linked immunosorbent assay (ELISA) was performed to detect and quantitatively analyze the amount of HMGB1 released from the cells following PEDOT NP-PTT. This immunoassay utilizes a capture and a detection antibody to immobilize and enable detection of a target antigen using highly specific antibody-antigen interactions. Briefly, after the 30 min incubation period at 37 °C following laser irradiation, cells were transferred to microcentrifuge tubes, centrifuged, and 80  $\mu$ L of the supernatant was analyzed using an HMGB1 Detection ELISA Kit (Chondrex, 6010). Antibodies and reagents were prepared per manufacturer's recommendations. Samples were mixed with dilution buffer in a 1:1 volume ratio. The absorbance at 450 nm of the samples was read with a Biotek H4 multimode plater reader using a 96-well plate.

### **3.9 Activation of Dendritic Cells (DCs)**

Immature JAWSII DCs were seeded in a 24-well transwell co-culture plate using sample volumes of 600  $\mu$ L and a cell density of 190,000 cells/well. DCs were incubated at 37 °C with 5% CO<sub>2</sub> for 72 h to allow for cellular adhesion. Separately and 48 h after DC incubation, B16-F10 melanoma cells were seeded in a transwell co-culture plate insert at a cell density of 250,000 cells/well and sample volumes of 100  $\mu$ L, then

incubated at 37 °C for 24 h. Afterwards, B16-F10 cell media was replaced with 100  $\mu$ L of PEDOT NP suspension at a concentration of 500  $\mu$ g/mL. After 1.5 h incubation with PEDOT NPs, plate inserts were transferred to wells in transwell plates containing DCs. B16-F10 cells were irradiated with 808-nm diode laser (3.0 W/cm<sup>2</sup>) for 5, 10, and 15 min. Co-cultured DCs and B16-F10 cells were incubated at 37 °C with 5% CO<sub>2</sub> for 48 h. After incubation, DCs were trypsinized, pelleted by centrifugation at 1000 rpm for 10 min, washed with DBPS (without Ca<sup>2+</sup> and Mg<sup>2+</sup>), and resuspended in 1% w/v BSA for 30 min to block non-specific binding. Following the 30 min incubation time, cells were centrifuged and BSA solution was discarded. DCs were incubated at 4 °C for 30 min with 50  $\mu$ L containing the conjugated monoclonal antibodies: APC anti-mouse CD11c (N418, 1:1600 dilution in 0.1% w/v BSA), PE anti-mouse CD80 (B7-1, 1:1600 dilution in 0.1% w/v BSA), and FITC anti-mouse CD86 (B7-2, 1:250 dilution in 0.1% w/v BSA) (Tonbo Biosciences, San Diego, CA, USA). DCs were washed, centrifuged, resuspended in DPBS, and analyzed by flow cytometry using a CytoFlex S Flow Cytometer (Beckman Coulter, Brea, CA, USA). Flow cytometry data was analyzed using the CytExpert software. The FITC, APC, and PE channels were selected to detect the fluorescence from the conjugated antibodies. Histograms illustrating the fluorescent intensity against cell count were plotted.

## 4. RESULTS

### 4.1 Characterization of PEDOT and PEDOT/NR NPs

The PEDOT NPs synthesized using the oxidative-emulsion polymerization method produced a NP suspension that was dark green with a dark blue hue (Figure 7A). The absorption spectra of the filtered PEDOT NP suspension revealed an absorbance between 700–1000 nm (NIR region) with a peak at 765 nm (Figure 7B). Dynamic light scattering (DLS) determined the filtered PEDOT NPs to have an average diameter size of  $27.15 \pm 0.32$  nm and a polydispersity index (PDI) of  $0.213 \pm 0.001$  (Figure 7C and Table 1). The PDI is calculated by dividing the mean size by the standard deviation of the NPs in a suspension and is representation of the distribution of size populations in a sample. A  $\text{PDI} > 0.7$  indicates a broad NP size distribution and  $\text{PDI} < 0.3$  indicates a homogenous population of NPs. Zeta potential analysis results are shown in Figure 7D. Filtered PEDOT NPs were found to have an average zeta potential of  $-38.3 \pm 1.75$  mV. The zeta potential is an indicator of the stability of colloidal dispersions measuring the magnitude of electrostatic repulsion between similarly charged particles. The high zeta potential confers stability, i.e., the NPs will resist aggregation.

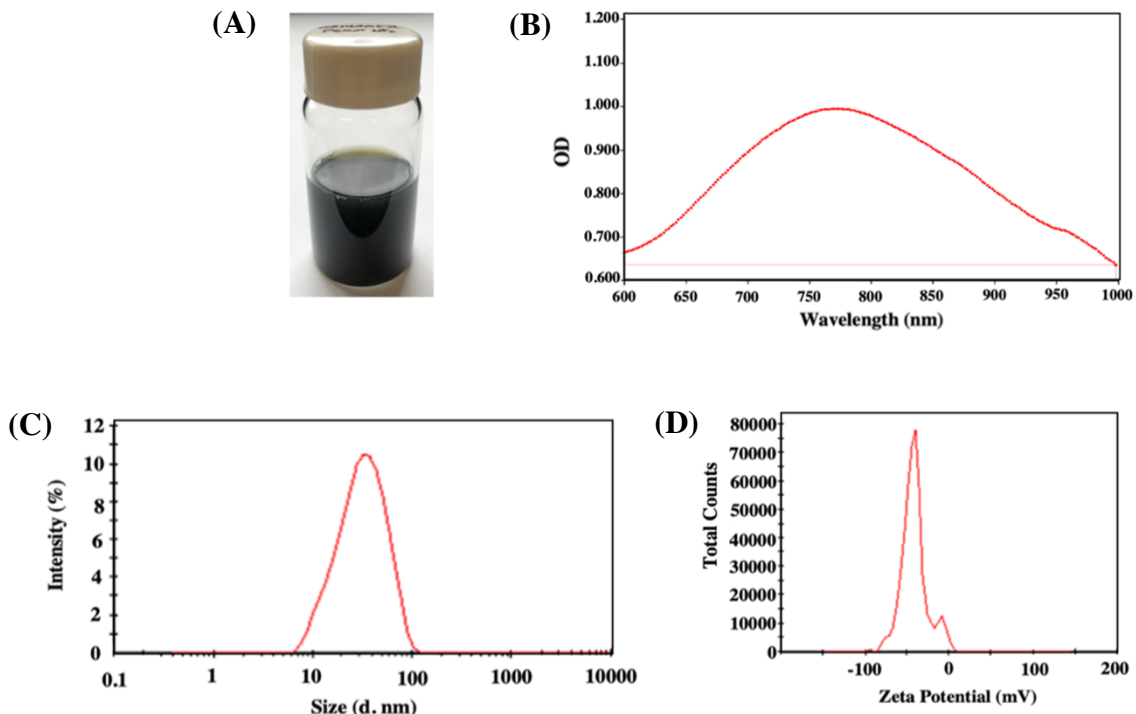


**Figure 7.** PEDOT NP characterization. (A) PEDOT NP suspension. (B) UV/VIS absorbance spectrum with peak absorbance at 765 nm. (C) Size distribution of NPs determined by DLS. (D) Zeta potential distribution of PEDOT NPs.

Filtered PEDOT/NR NPs, synthesized for visualization of cellular uptake by B16F10 cells, were characterized and found to have an average diameter size of  $55.22 \pm 1.44$  nm, PDI value of  $0.136 \pm 0.041$ , and a zeta potential of  $-50.4 \pm 1.58$ , as shown in Figure 8 and Table 1.

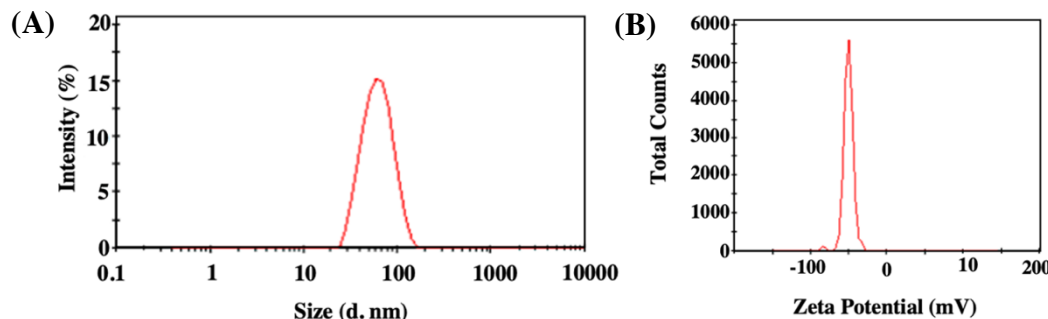


**Figure 8.** PEDOT/NR NP characterization. (A) Size distribution determined by DLS. (B) Zeta potential distribution of PEDOT/NR NPs.

**Table 1.** Filtered PEDOT and PEDOT/NR Size, PDI, and Zeta Potential. Standard deviations were calculated from three measurements of the same batch of NPs.

NPs	Size (nm)	PDI	Zeta Potential (mV)
<b>PEDOT</b>	$27.15 \pm 0.32$	$0.213 \pm 0.001$	$-38.3 \pm 1.75$
<b>PEDOT/NR</b>	$55.22 \pm 1.44$	$0.136 \pm 0.041$	$-50.4 \pm 1.58$

#### 4.2 Analysis of PEDOT NPs as Photothermal Agents

The Seek Shot™ thermal camera was utilized to both measure and visualize the change in temperature in real-time. The thermal images in Figure 9A show the temperature increase of a  $100\text{-}\mu\text{L}$  sample containing  $500\text{ }\mu\text{g/mL}$  of PEDOT NPs upon irradiation with an 808-nm laser diode at  $3.0\text{ W/cm}^2$  for 15 min. The temperature of three independent PEDOT NP suspensions in media at  $500\text{ }\mu\text{g/mL}$  was measured with the maximum temperature reaching  $64\text{ }^\circ\text{C}$  (i.e.  $\sim 42\text{ }^\circ\text{C}$  above room temperature). The graph in Figure 9B shows the temperature increase as a function of time demonstrating the PEDOT NPs photothermal properties and their ability to elevate the temperature by almost  $40\text{ }^\circ\text{C}$ . The graph in Figure 9B also shows that a steep increase in temperature occurs within the first 4 min before it plateaus with minimal temperature change occurring between 5 and 15 min. There was no temperature change in control samples lacking PEDOT NPs during the 15 min laser irradiation.

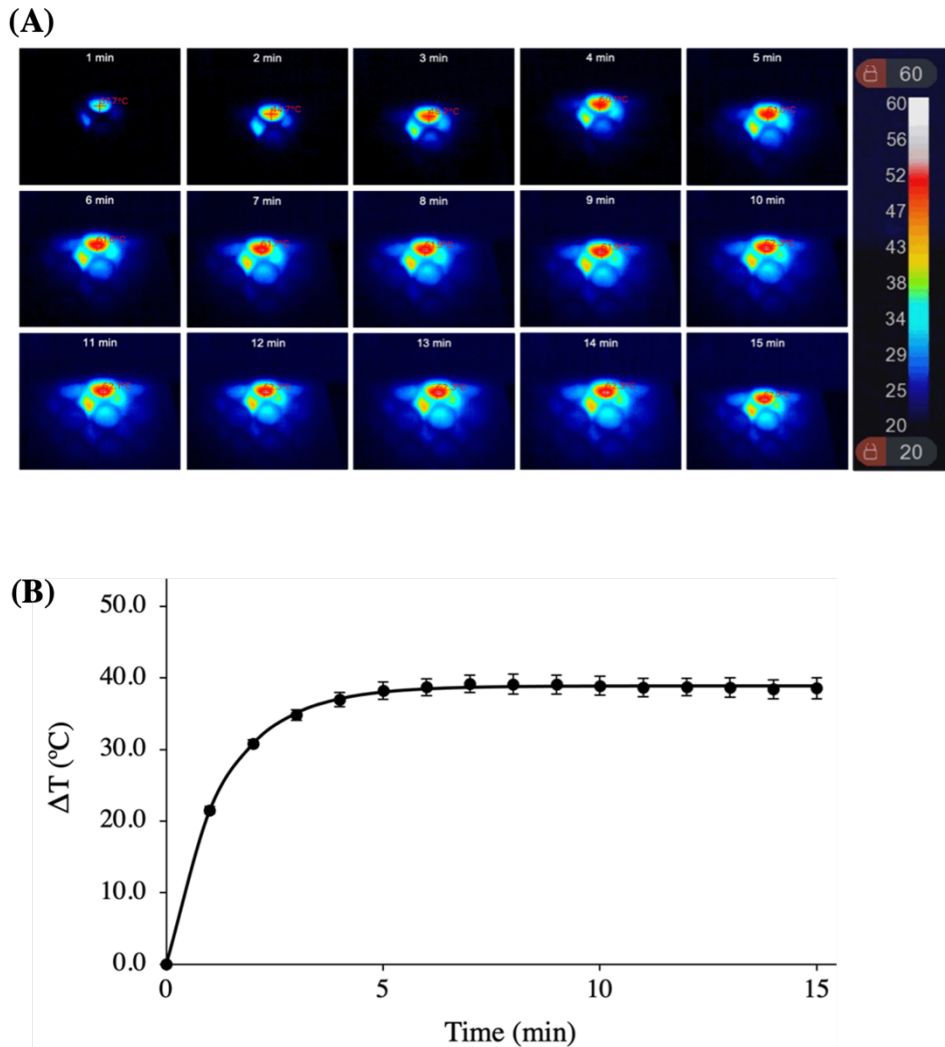


**Figure 9.** Temperature (°C) change over 15 min time period. (A) Thermal images of PEDOT NP suspension (500  $\mu\text{g}/\text{mL}$ ) in media being irradiated with 808-nm laser diode (3.0  $\text{W}/\text{cm}^2$ ) for 15 min. (B) Change in temperature ( $\Delta T$ ) as a function of time (min) for PEDOT NP suspension (500  $\mu\text{g}/\text{mL}$ ) in cell media upon irradiation with an 808-nm laser diode (3.0  $\text{W}/\text{cm}^2$ ). Curve was fitted using a non-linear least squares model. Error bars represent the standard deviation between three independent replicates ( $n = 3$ ).

#### **4.3 Intracellular Localization of PEDOT NPs**

The cellular uptake and localization of PEDOT NPs containing Nile Red (PEDOT/NR NPs) in B16-F10 melanoma cells after a 1.5 h incubation period was observed using an Olympus® FLUOVIEW FV3000 confocal laser scanning microscope. Figure 9 displays the results from the fluorescence microscopy. The cell nucleus stained with DAPI fluoresced blue (Figure 10A and 10D) and the tubulin cytoskeleton stained with DyLight® 488 fluoresced green (Figure 10B and 10D). Although, it was observed in that the tubulin stain did not reveal the normal morphology of the actin filaments (Figure 10B). PEDOT/NR NPs were able to diffuse into the B16-F10 cells which was detected as red fluorescence (Figure 10C and 10D). As expected, PEDOT/NR NPs accumulated mainly in the cytoplasm with no fluorescence detected inside the nucleus. These observations confirm the ability of the PEDOT NPs to be actively transported into the cell via the endocytic pathway where they can carry out their function as photothermal agents.

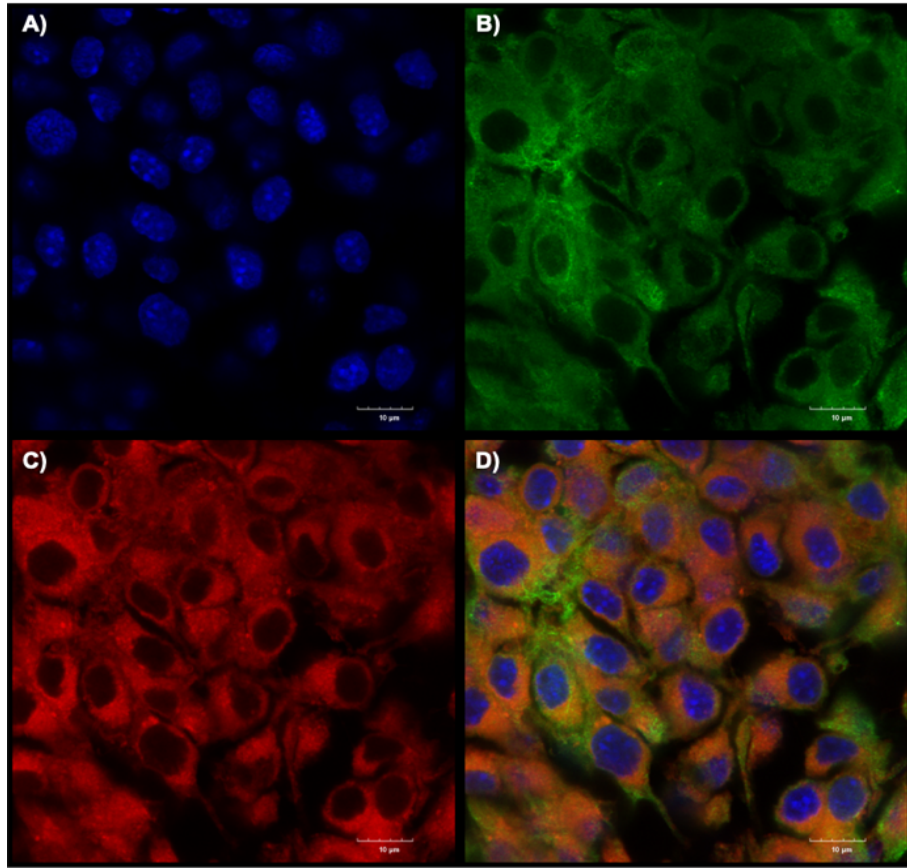


**Figure 10.** Laser scanning confocal microscopy images of B16-F10 melanoma cancer cells incubated with PEDOT/NR NPs at a  $500 \mu\text{g/mL}$  concentration for 1.5 h. (A) Cell nucleus stained with DAPI, (B) Actin filaments stained with anti-tubulin antibody, (C) Nile Red encapsulated within PEDOT NPs, (D) overlay of all the images. Scale bar =  $10 \mu\text{m}$ .

#### 4.4 Qualitative Analysis of Cell Death by MTT Assay

The effect of PEDOT NP-PTT on cell death was qualitatively analyzed as a function of laser irradiation time using the MTT assay. Figure 11 shows the results of cell viability after 5-, 10-, and 15-min exposure to NIR laser irradiation. Cell viability was greatly decreased in cells that were treated with PEDOT NPs and exposed to NIR laser irradiation compared to the control groups: NP control (cells exposed to PEDOT

NPs but not laser irradiation); Laser control (cells exposed to laser irradiation but not NPs); and NT (cells that did not receive any treatment). There was an unexpected decrease in cell viability of about 11% in the NP control which could be due to possible cytotoxicity. Cells irradiated for 10 and 15 min resulted in complete cell death with cell viability results similar to the positive control group of cells treated with MeOH for 15 min to induce cell death.

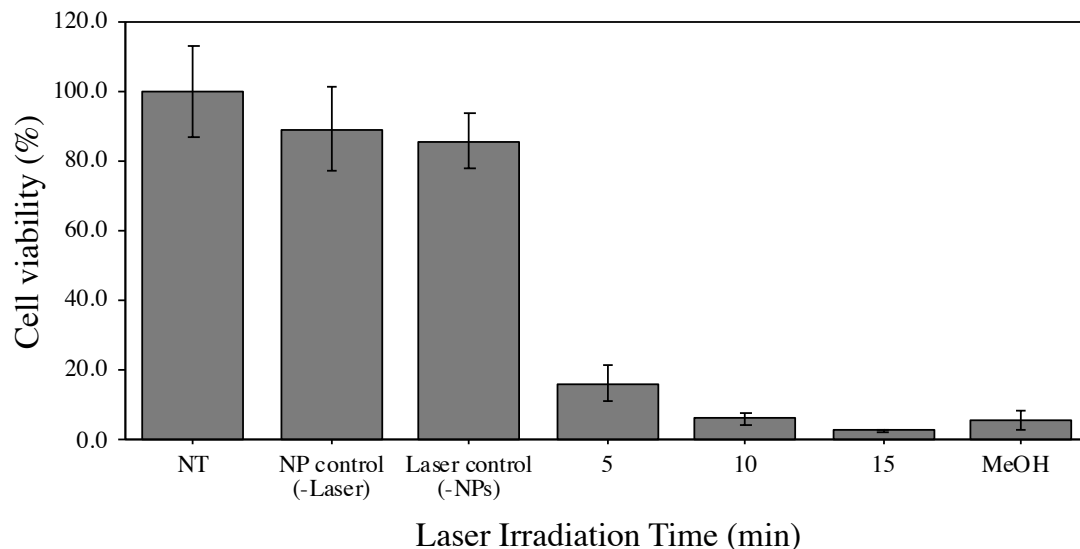


**Figure 11.** B16-F10 cell viability as a function of time. Cells were exposed to laser irradiation for 5, 10, and 15 min after 1.5 h incubation with PEDOT NPs at a concentration of 500  $\mu$ g/mL. Controls include cells without treatment (NT); NP control: cells with PEDOT NPs but not exposed to laser irradiation (-Laser); cells exposed to 15-min laser irradiation without NPs (-NPs); MeOH: cells treated with MeOH for 15 min. Bars represent the mean  $\pm$  SD ( $n = 3$ ).

#### 4.5 Presentation of Damage Associated Molecular Patterns (DAMPs)

The expression of DAMPs on the surface of the B16-F10 cells following PEDOT NP-PTT was investigated by flow cytometry which quantitatively analyzed the level of

surface bound high-mobility group box 1 (HMGB1), calreticulin (CRT), heat-shock protein 70 (HSP70), and heat-shock protein 90 (HSP90). Flow cytometry data was done as just one study with one sample per condition. The histograms in Figure 12 show the fluorescence intensities associated with the expression of each DAMP: CRT (A), HMGB1 (B), HSP70, and HSP90 (D) for each study. The level of DAMP expression increased in all of the cell groups treated with PEDOT NPs and exposed to NIR laser (0-15 min) which can be seen by the fluorescent intensities increasing and shifting to the right compared to the control groups. Figure 12 also shows that the level of DAMP expression did not increase when cells were treated with NIR laser irradiation alone (green data set) and, in fact, stayed the same as the no treatment (NT) group (red data set). Unexpectedly, DAMP expression increased in cells treated with PEDOT NPs but not exposed to NIR laser irradiation (pink data set). The scatter plots show a change in cell size and granularity in samples of cells treated with NIR laser irradiation compared to the control groups (Appendix Figure 1A).

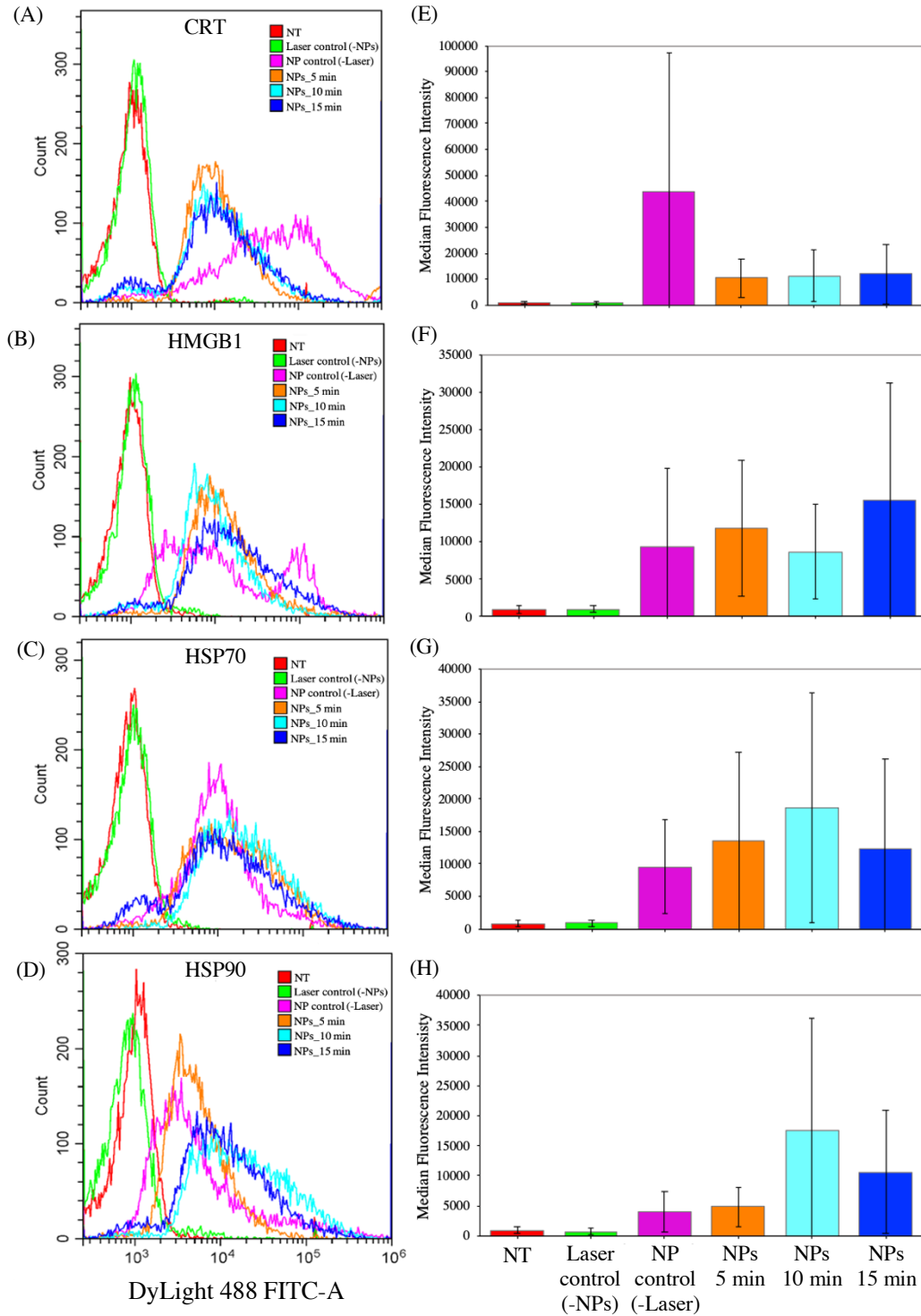


**Figure 12.** Flow cytometry histograms. Surface bound DAMPs, (A, E) Calreticulin (CRT), (B, F) HMGB1, (C, G) HSP70, and (D, H) HSP90 after 5-, 10-, and 15-min laser irradiation. Error bars represent the robust standard deviation (rSD) between the median fluorescence intensity of 10,000 cells.

The release of DAMPs from the cells following PEDOT NP-PTT was investigated using the HMGB1 ELISA Detection Kit (6010) which quantitatively analyzed the amount of HMGB1 present in the cell media (Figure 13). As expected, the least amount of HMGB1 was detected in the cell media obtained from cells that received no treatment (NT) and cells exposed to NIR laser irradiation alone without NPs (Laser control). The largest amount of released HMGB1 was detected from cells exposed to 10 min of NIR laser irradiation, which was also an increase of 275% compared to cells exposed to 5 min of laser irradiation. It was also noted that the amount of HMGB1 was greater in cells that were not exposed to laser irradiation (NP control) than cells exposed to laser irradiation for 5 min.

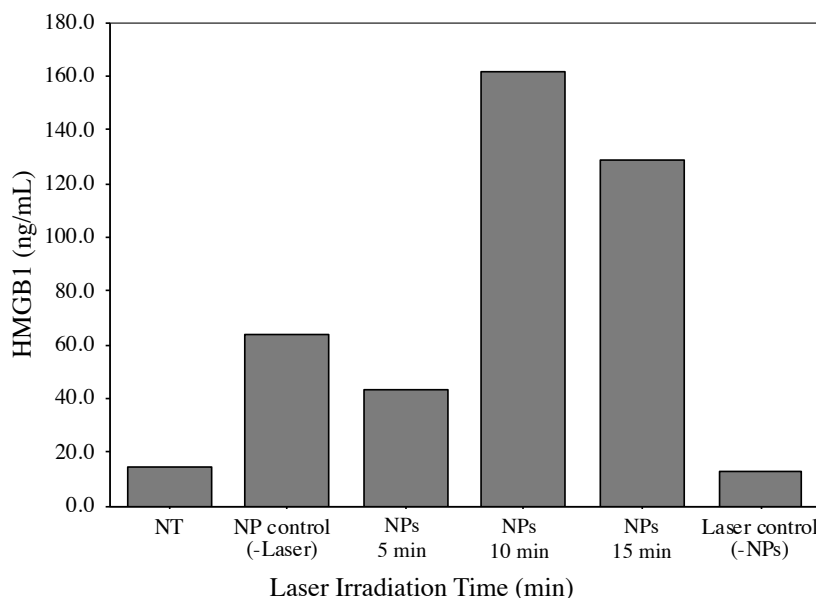


**Figure 13.** Amount of HMGB1 (ng/mL) detected in cell media after 5-, 10-, and 15-min laser irradiation. Controls include media from cells without treatment (NT), NP control: cells with PEDOT NPs but not exposed to laser (-Laser), and Laser control: cells exposed to 15-min laser irradiation but without PEDOT NPs (-NPs).

#### **4.6 Dendritic Cell (DC) Activation**

The activation of DCs by DAMPs released from B16-F10 cells was investigated by flow cytometry, which analyzed the level of expressed DC surface markers. The histograms in Figure 14 show the fluorescence intensities associated with the expression of the DC surface markers for each study: CD11c (A), CD80 (B), and CD86 (C). In these figures, peak intensity is associated with the number of cells presenting a given fluorescence intensity. The location of the peak on the x axis, on the other hand, indicates the level of fluorescence for a given population of cells. Figure 14 shows the data collected for the gates (A) APC, (B) PE, and (C) FITC. Figure 14 shows a disproportionate number of DCs co-cultured with B16-F10 cells exposed to laser irradiation for 10 min (light blue peak) and 15 min (blue peak) and can be seen for CD11c, CD80, and CD86. This was a result of that an experimental error that occurred during the flow cytometer's cell counting process which caused an uneven number of events to be recorded for the samples. Figure 14 also shows a decrease in the fluorescent intensities of CD11c and CD80 which can be seen by the fluorescent intensities shifting to the left compared to the control groups: NT (red peak), NP control (green peak), and Laser control (pink peak). Scatter plots revealed a change in cell size and granularity in samples of cells treated with NIR laser irradiation compared to the control groups; similar to what was observed in the DAMP studies (Appendix Figure 2A). Future studies will focus on optimizing the conjugated antibody staining procedure that will include adjusting the dilution ratios to improve target recognition and antibody attachment. Also, a positive control will be incorporated in future studies that will consist of mature DCs that will be activated by lipopolysaccharides.

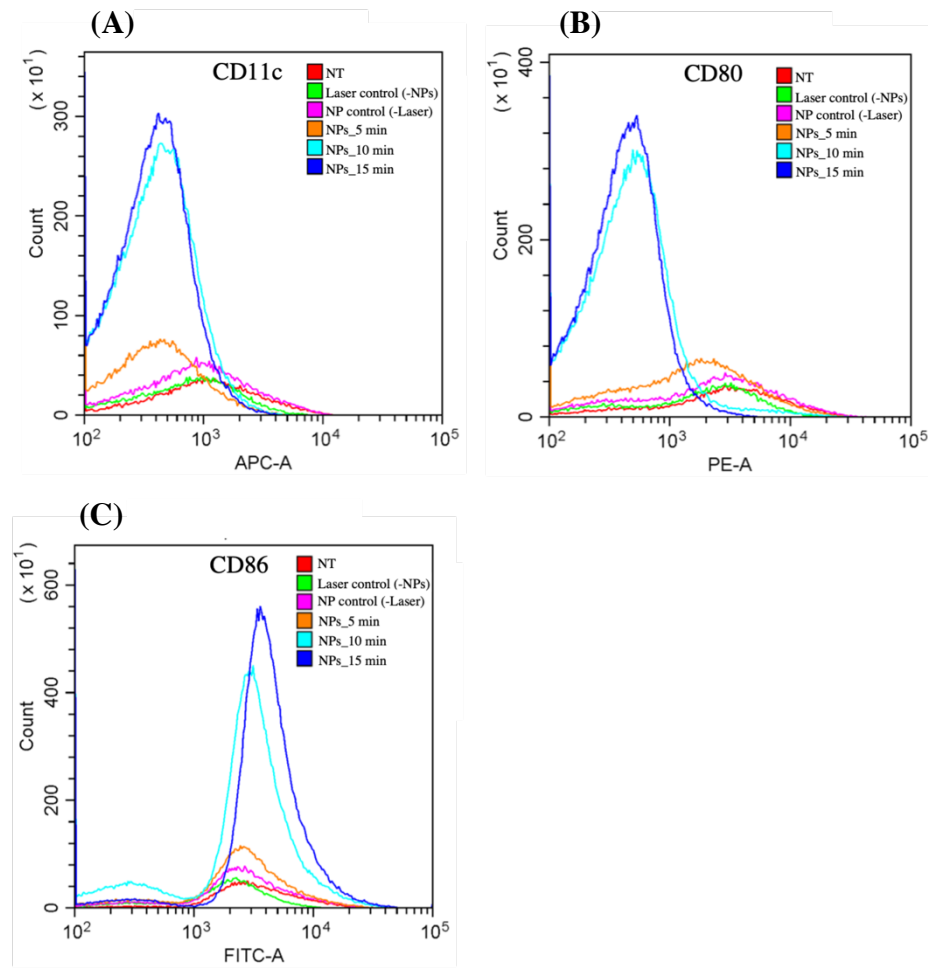


**Figure 14.** Fluorescence intensities of DC markers. (A) CD11c, (B) CD80, and (C) CD86 detected on the surface of DCs after 48 h incubation with laser irradiated B16-F10 cells and control samples.

## 5. DISCUSSION AND CONCLUSION

### 5.1 Discussion

In this work, we synthesized conductive PEDOT NPs from the monomer 3,4-ethylenedioxythiophene (EDOT) using an oxidative-emulsion polymerization process. Synthesized NPs were characterized and confirmed to be within the desired size of less than 100 nm to allow them to diffuse through the tumor tissue efficiently but were smaller than those used in our previous work (Cantu *et al.* and Huff *et al.*).<sup>9,10</sup> The negative zeta potential of the NPs contributed to their colloidal stability due to the high magnitude of electrostatic repulsion between NPs. The negative zeta potential obtained verified the interactions between the anionic surfactants with the positively charged polymer. Although the absorbance spectra of the NPs confirmed their ability to absorb light in the NIR region, their absorbance value was lower than the ones previously reported by Cantu *et al.* and Huff *et al.* from our laboratory.<sup>9,10</sup> It is important to note that the PEDOT NP preparation process is known to lead to significant variations between batches like the ones observed in these studies.

Images obtained from the cellular internalization of the PEDOT/NR NPs revealed that the DyLight 488 stain did not show the normal morphology of the actin filaments (Figure 9B). This suggests that either the antibody used was no longer stable or perhaps the cells were overstained. Another discrepancy found in our data was in the distribution of the PEDOT/NR NPs within the cells, which differed than that observed by Huff *et al.* in MDA-MD-231 breast cancer cells.<sup>10</sup> Instead of seeing the accumulation in round vesicles, indicating possible localization within endosomes, we saw diffuse distribution

throughout. A possible reason for this could be that Nile Red might not actually be encapsulated within the NPs causing it to diffuse into the cells as a small molecule. Another possibility is that the Nile Red prematurely diffused from the NPs and into the cells. A final possibility is that the smaller size of the NPs relative to our prior work allowed the NPs to enter the cells nonspecifically. It is important to mention that the PEDOT/NR NPs used in this study were prepared only once as opposed to PEDOT NPs which were synthesized many times.

B16-F10 melanoma cancer cell were used as the *in vitro* model of cancer for the experimental studies. Malignant melanoma is the sixth most common cancer in the U.S. Although less common than other types of skin cancer, if not caught early, it is more dangerous due to its ability to metastasize to other parts of the body. Patients with malignant melanoma are currently being treated with ICP therapy.<sup>13</sup> Therefore, the work accomplished in this thesis towards the effectiveness of PEDOT NP-PTT with this cell line is important.

A goal in this study was to analyze the effect of PEDOT NP-PTT on cell death to gain insight in this localized treatment of cancer. Based on our previous published work, we hypothesized that PEDOT NP within melanoma cells would lead to activated cell death as a result of laser induced hyperthermia. Parameters used in this study such as the PEDOT NP concentration, NP-cell incubation time, and laser irradiation time were based on our previous work (Huff *et al.*) that investigated the modification of these parameters.<sup>10</sup> The unexpected decrease observed in the cell viability in our NP control group was based on our prior published data by Cantu *et al.* and Huff *et al.*, which utilized MDA-MB-231 breast cancer cells.<sup>9,10</sup> The resulting reduction in cell viability

could potentially be attributed to a cell type-specific sensitivity to the PEDOT NPs or to the smaller size of the NPs.

Another major goal of this study was to analyze the induction of immunogenic cell death (ICD) in response to PEDOT NP-PTT. Damage-associated molecular patterns (DAMPs) secreted by apoptotic cells can initiate an adaptive immune response.<sup>19</sup> Based on our previously published work (Huff *et al.*), PEDOT NP-PTT was shown to be able to elicit an apoptotic cell death in MDA-MB-231 breast cancer cells through the upregulation of caspase-3/7.<sup>10</sup> The flow cytometry data from this study revealed an increase in DAMP expression for CRT, HMGB1, HSP70, and HSP90 in response to both PEDOT NP exposure and PTT, as opposed to PTT alone. Similar results were obtained from the ELISA data for HMGB1 released from B16-F10 cells. Thus, showing the ability of PEDOT NP-PTT to evoke an ICD pathway in B16-F10 melanoma cells.

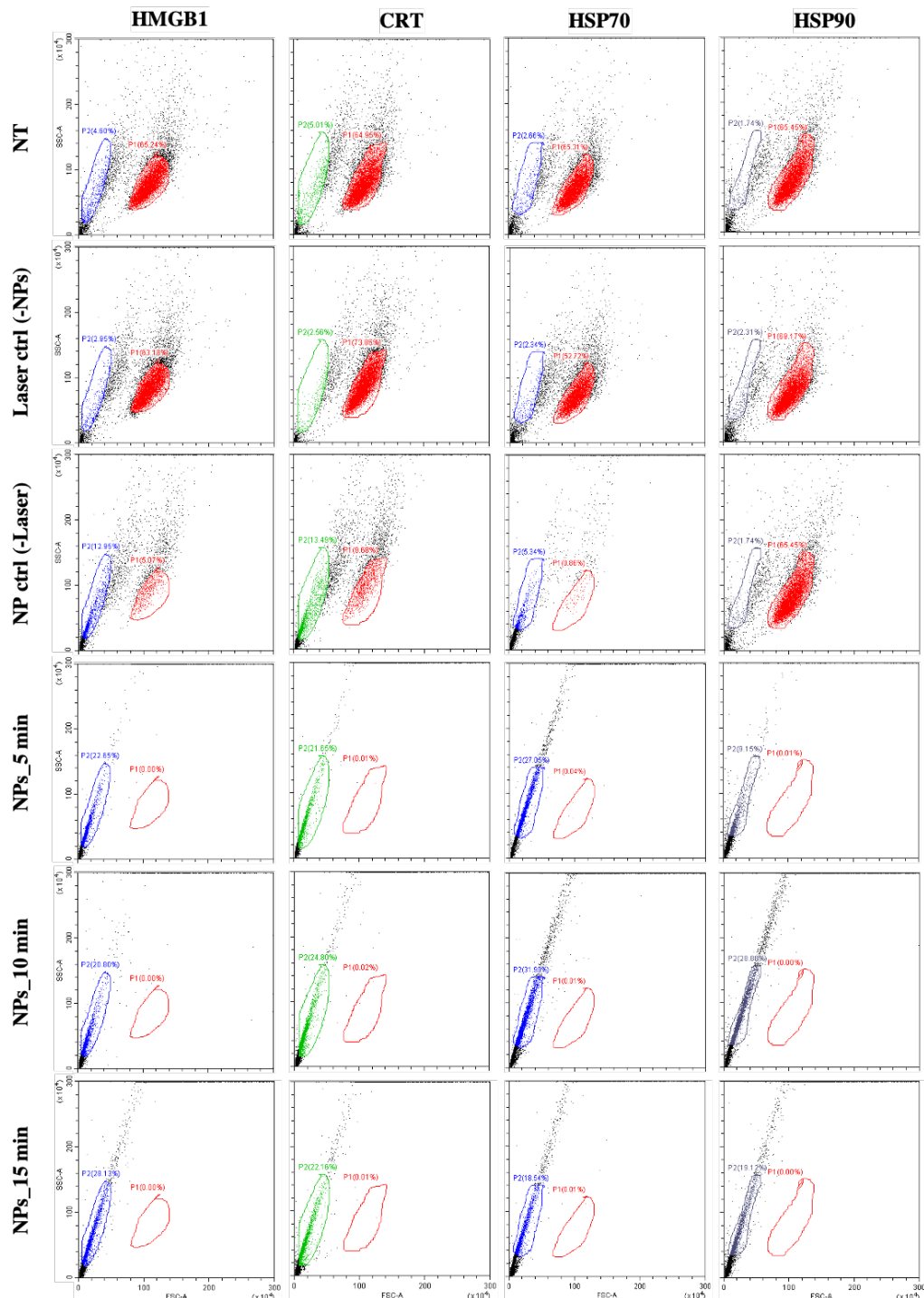
The activation of dendritic cells (DCs) was another major goal of this study. Translocated DAMPs can stimulate an antitumor immune response by binding to receptors on the surface of DCs, thereby activating them and causing them to engulf the dying cancer cells.<sup>46</sup> In a study similar to ours, Nguyen *et al.* reported dendritic cell activation with the presence of DAMP signals released from MDA-MB-231 breast cancer cells after laser irradiation.<sup>47</sup> Unfortunately, the flow cytometry data collected from this study proved to be unsuccessful. The irregularity in the fluorescence intensities suggests that cell staining did not work well. Future studies will focus on optimizing the conjugated antibody staining procedure that will include adjusting the dilution ratios to improve target recognition and antibody attachment. Also, a positive control will be incorporated in future studies that will consist of mature DCs that will be activated by

lipopolysaccharides (LPS), as reported by Nguyen *et al.*<sup>47</sup>

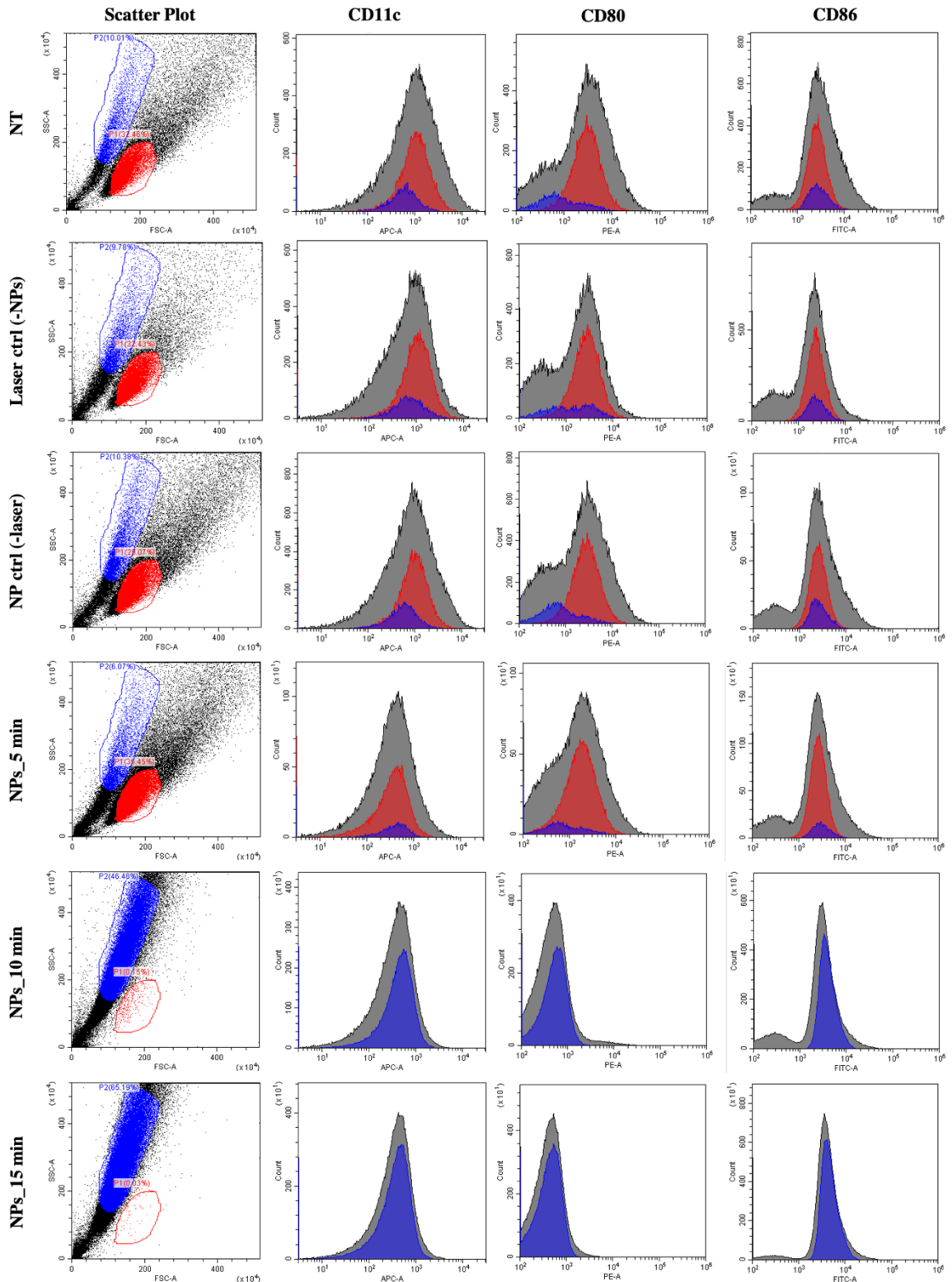
## 5.2 Conclusion

PEDOT NPs synthesized were confirmed to be within the optimal size of less than 100 nm, as confirmed by dynamic light scattering and displayed the ability to absorb light in the NIR region. The PEDOT NPs proved to be effective photothermal agents able to create a maximum change in temperature of approximately 40 °C; enough to cause cell death after 5 min of laser irradiation at a concentration of 500 µg/mL. Flow cytometry and ELISA assays revealed the induction of immunogenic cell death following PEDOT NP-PTT, with the increase of calreticulin, HMGB1, HSP70, and HSP90 detected as a result of 0-, 5-, 10-, and 15-min laser irradiation. Despite some promising results, not all of the goals in this study were reached mostly due to the unprecedented global pandemic. The work from these studies does, however, identify experimental parameters that need to be addressed and reevaluated in order to optimize the efficacy of this treatment for future studies.

## APPENDIX SECTION



**Appendix Figure A1.** Flow cytometry scatter plots of DAMPs. Side scatter (SSC) versus forward scatter (FSC) plots of HMGB1, CRT, HSP70, and HSP90 for each experimental parameter with two cell populations gated.



**Appendix Figure A2.** Flow cytometry scatter plots and fluorescence intensity histograms of DC markers. Gates created around two population of cells and color coded blue and red (scatter plots). The fluorescence intensities of the two cell populations (red and blue histograms) detected in the fluorescence intensity of CD11c, CD80, and CD86 (grey).

## REFERENCES

1. Heron, M., Hoyert, D. L., Murphy, S. L., Xu, J., Kochanek, K. D., and Tejeda-Vera, B. (2009) Deaths: Final Data for 2006. *Natl. Vital Stat. Reports.* **57**, 1–136
2. Jemal, A., Siegel, R., Ward, E., Hao, Y., Xu, J., Murray, T., and Thun, M. J. (2008) Cancer Statistics, 2008. *CA. Cancer J. Clin.* **58**, 71–96
3. Siegel, R. L., Miller, K. D., and Jemal, A. (2020) Cancer statistics, 2020. *CA. Cancer J. Clin.* **70**, 7–30
4. Dobry, A. S., Zogg, C. K., Hodi, F. S., Smith, T. R., Ott, P. A., and Iorgules, J. B. (2018) Management of metastatic melanoma: improved survival in a national cohort following the approvals of checkpoint blockade immunotherapies and targeted therapies. *Cancer Immunol. Immunother.* **67**, 1833–1844
5. Domingues, B., Lopes, J., Soares, P., and Populo, H. (2018) Melanoma treatment in review. *ImmunoTargets Ther.* **7**, 35–49
6. Widakowich, C., de Castro, G., de Azambuja, E., Dinh, P., and Awada, A. (2007) Review: Side Effects of Approved Molecular Targeted Therapies in Solid Cancers. *Oncologist.* **12**, 1443–1455
7. Sharma, P., A. J. P. (2015) The Future of Immune Checkpoint Therapy. *Science (80-. ).* **348**, 56–61
8. Marin-Acevedo, J. A., Dholaria, B., Soyano, A. E., Knutson, K. L., Chumsri, S., and Lou, Y. (2018) Next generation of immune checkpoint therapy in cancer: New developments and challenges. *J. Hematol. Oncol.* **11**, 1–20

9. Cantu, T., Walsh, K., Pattani, V. P., Moy, A. J., Tunnell, J. W., Irvin, J. A., and Betancourt, T. (2017) Conductive polymer-based nanoparticles for laser-mediated photothermal ablation of cancer: Synthesis, characterization, and in vitro evaluation. *Int. J. Nanomedicine.* **12**, 615–632
10. Huff, M. E., Gökm̄en, F. Ö., Barrera, J. S., Lara, E. J., Tunnell, J., Irvin, J., and Betancourt, T. (2020) Induction of Immunogenic Cell Death in Breast Cancer by Conductive Polymer Nanoparticle-Mediated Photothermal Therapy. *ACS Appl. Polym. Mater.* 10.1021/acsapm.0c00938
11. Sharma, P., and Allison, J. P. (2015) Immune checkpoint targeting in cancer therapy: Toward combination strategies with curative potential. *Cell.* **161**, 205–214
12. Eno, J. (2017) Immunotherapy Through the Years. *J. Adv. Pract. Oncol.* **8**, 747–753
13. Pardoll, D. M. (2012) The blockade of immune checkpoints in cancer immunotherapy. *Nat. Rev. Cancer.* **12**, 252–264
14. Darvin, P., Toor, S. M., Sasidharan Nair, V., and Elkord, E. (2018) Immune checkpoint inhibitors: recent progress and potential biomarkers. *Exp. Mol. Med.* **50**, 1–11
15. Sharma, P., Hu-Lieskován, S., Wargo, J. A., and Ribas, A. (2017) Primary, Adaptive, and Acquired Resistance to Cancer Immunotherapy. *Cell.* **168**, 707–723
16. Moy, A. J., and Tunnell, J. W. (2017) Combinatorial immunotherapy and nanoparticle mediated hyperthermia. *Adv. Drug Deliv. Rev.* **114**, 175–183

17. Elmore, S. (2007) Apoptosis: A Review of Programmed Cell Death. *Toxicol. Pathol.* **35**, 495–516
18. Zhivotovsky, B., and Orrenius, S. (2010) Cell cycle and cell death in disease: Past, present and future. *J. Intern. Med.* **268**, 395–409
19. Galluzzi, L., Vitale, I., Aaronson, S. A., Abrams, J. M., Adam, D., Agostinis, P., et al. (2018) Molecular mechanisms of cell death: Recommendations of the Nomenclature Committee on Cell Death 2018. *Cell Death Differ.* **25**, 486–541
20. Zhou, J., Wang, G., Chen, Y., Wang, H., Hua, Y., and Cai, Z. (2019) Immunogenic cell death in cancer therapy: Present and emerging inducers. *J. Cell. Mol. Med.* **23**, 4854–4865
21. Obeid, M., Tesniere, A., Ghiringhelli, F., Fimia, G. M., Apetoh, L., Perfettini, J. L., et al. (2007) Calreticulin exposure dictates the immunogenicity of cancer cell death. *Nat. Med.* **13**, 54–61
22. Michaud, M., Martins, I., Sukkurwala, A. Q., Adjemian, S., Ma, Y., Pellegatti, et al. (2011) Autophagy-dependent anticancer immune responses induced by chemotherapeutic agents in mice. *Science (80-. ).* **334**, 1573–1577
23. Bell, C. W., Jiang, W., Reich, C. F., and Pisetsky, D. S. (2006) The extracellular release of HMGB1 during apoptotic cell death. *Am. J. Physiol. - Cell Physiol.* **291**, 1318–1325

24. Kalinina, N., Agrotis, A., Antropova, Y., DiVitto, G., Kanellakis, P., Kostolias, G., Ilyinskaya, O., Tararak, E., and Bobik, A. (2004) Increased expression of the DNA-binding cytokine HMGB1 in human atherosclerotic lesions: Role of activated macrophages and cytokines. *Arterioscler. Thromb. Vasc. Biol.* **24**, 2320–2325
25. Apetoh, L., Ghiringhelli, F., Tesniere, A., Obeid, M., Ortiz, C., Criollo, A., et al. (2007) Toll-like receptor 4-dependent contribution of the immune system to anticancer chemotherapy and radiotherapy. *Nat. Med.* **13**, 1050–1059
26. Garg, A. D., Krysko, D. V., Vandenabeele, P., and Agostinis, P. (2012) Hypericin-based photodynamic therapy induces surface exposure of damage-associated molecular patterns like HSP70 and calreticulin. *Cancer Immunol. Immunother.* **61**, 215–221
27. Buytaert, E., Dewaele, M., and Agostinis, P. (2007) Molecular effectors of multiple cell death pathways initiated by photodynamic therapy. *Biochim. Biophys. Acta - Rev. Cancer.* **1776**, 86–107
28. Sweeney, E. E., Cano-Mejia, J., and Fernandes, R. (2018) Photothermal Therapy Generates a Thermal Window of Immunogenic Cell Death in Neuroblastoma. *Small.* **14**, 1–8
29. Chenthamara, D., Subramaniam, S., Ramakrishnan, S. G., Krishnaswamy, S., Essa, M. M., Lin, F. H., and Qorongfleh, M. W. (2019) Therapeutic efficacy of nanoparticles and routes of administration. *Biomater. Res.* **23**, 1–29

30. Baetke, S. C., Lammers, T., and Kiessling, F. (2015) Applications of nanoparticles for diagnosis and therapy of cancer. *Br. J. Radiol.* 10.1259/bjr.20150207
31. Ledet, G., and Mandal, T. K. (2012) Nanomedicine : Emerging Therapeutics for the 21st Century. *US Pharm.*
32. Ventola, C. L. (2012) The nanomedicine revolution: Part 2: Current and future clinical applications. *P T.* **37**, 582–591
33. Alexis, F., Pridgen, E., Molnar, L. K., and Farokhzad, O. C. (2008) Factors affecting the clearance and biodistribution of polymeric nanoparticles. *Mol. Pharm.* **5**, 505–515
34. Adiseshaiah, P. P., Hall, J. B., and McNeil, S. E. (2010) Nanomaterial standards for efficacy and toxicity assessment. *Wiley Interdiscip. Rev. Nanomedicine Nanobiotechnology.* **2**, 99–112
35. Bharali, D. J., and Mousa, S. A. (2010) Emerging nanomedicines for early cancer detection and improved treatment: Current perspective and future promise. *Pharmacol. Ther.* **128**, 324–335
36. Morigi, V., Tocchio, A., Bellavite Pellegrini, C., Sakamoto, J. H., Arnone, M., and Tasciotti, E. (2012) Nanotechnology in Medicine: From Inception to Market Domination. *J. Drug Deliv.* **2012**, 1–7
37. Wilhelm, S., Tavares, A. J., Dai, Q., Ohta, S., Audet, J., Dvorak, H. F., and Chan, W. C. W. (2016) Analysis of nanoparticle delivery to tumours. *Nat. Rev. Mater.* 10.1038/natrevmats.2016.14

38. Arranja, A. G., Pathak, V., Lammers, T., and Shi, Y. (2017) Tumor-targeted nanomedicines for cancer theranostics. *Pharmacol. Res.* **115**, 87–95
39. Kaur, P., Aliru, M. L., Chadha, A. S., Asea, A., and Krishnan, S. (2016) Hyperthermia using nanoparticles - Promises and pitfalls. *Int. J. Hyperth.* **32**, 76–88
40. Cabada, T. F., de Pablo, C. S. L., Serrano, A. M., Guerrero, F. del P., Olmedo, J. J. S., and Gomez, M. R. (2012) Induction of cell death in a glioblastoma line by hyperthermic therapy based on gold nanorods. *Int. J. Nanomedicine.* **7**, 1511–1523
41. Huang, X., Jain, P. K., El-Sayed, I. H., and El-Sayed, M. A. (2008) Plasmonic photothermal therapy (PPTT) using gold nanoparticles. *Lasers Med. Sci.* **23**, 217–228
42. Bhumkar, D. R., Joshi, H. M., Sastry, M., and Pokharkar, V. B. (2007) Chitosan reduced gold nanoparticles as novel carriers for transmucosal delivery of insulin. *Pharm. Res.* **24**, 1415–1426
43. Hwu, J. R., Lin, Y. S., Josephrajan, T., Hsu, M. H., Cheng, F. Y., Yeh, C. S., Su, W. C., and Shieh, D. Bin (2009) Targeted paclitaxel by conjugation to iron oxide and gold nanoparticles. *J. Am. Chem. Soc.* **131**, 66–68
44. Roy, I., Ohulchanskyy, T. Y., Pudavar, H. E., Bergey, E. J., Oseroff, A. R., Morgan, J., Dougherty, T. J., and Prasad, P. N. (2003) Ceramic-based nanoparticles entrapping water-insoluble photosensitizing anticancer drugs: A novel drug-carrier system for photodynamic therapy. *J. Am. Chem. Soc.* **125**, 7860–7865

45. Pantarotto, D., Singh, R., McCarthy, D., Erhardt, M., Briand, J. P., Prato, M., Kostarelos, K., and Bianco, A. (2004) Functionalized carbon nanotubes for plasmid DNA gene delivery. *Angew. Chemie - Int. Ed.* **43**, 5242–5246
46. Kroemer, G., Galluzzi, L., Kepp, O., and Zitvogel, L. (2013) Immunogenic cell death in cancer therapy. *Annu. Rev. Immunol.* **31**, 51–72
47. Nguyen, H. T. M., Katta, N., Widman, J. A., Takematsu, E., Feng, X., Torres, S. H., Betancourt, T., Baker, A. B., Suggs, L. J., Milner, T. E., and Tunnell, J. W. (2020) Laser nanobubbles induce immunogenic cell death in breast cancer. *bioRxiv*. 10.1101/2020.09.04.283846